PCP
PLANT & CELL PHYSIOLOGY

Special Issue – Regular Paper

Cannabis Glandular Trichome Cell Walls Undergo Remodeling to Store Specialized Metabolites

Samuel J. Livingston[1], Eun Jeong Bae[1], Faride Unda[2], Michael G. Hahn[3], Shawn D. Mansfield[2], Jonathan E. Page[1] and A. Lacey Samuels[1,*]

[1]Department of Botany, University of British Columbia, 6270 University Boulevard, Vancouver, BC V6T1Z4, Canada
[2]Department of Wood Science, University of British Columbia, 2424 Main Mall, Vancouver, BC V6T1Z4, Canada
[3]The Complex Carbohydrate Research Center, University of Georgia, 315 Riverbend Rd, Athens, GA 30602, USA

*Corresponding author: E-mail, lsamuels@mail.ubc.ca
(Received 15 May 2021; Accepted 13 August 2021)

The valuable cannabinoid and terpenoid metabolites of *Cannabis sativa* L. are produced by floral glandular trichomes. The trichomes consist of secretory disk cells, which produce the abundant lipidic metabolites, and an extracellular storage cavity. The mechanisms of apoplastic cavity formation to accumulate and store metabolites in cannabis glandular trichomes remain wholly unexplored. Here, we identify key wall components and how they change during cannabis trichome development. While glycome and monosaccharide analyses revealed that glandular trichomes have loosely bound xyloglucans and pectic polysaccharides, quantitative immunolabeling with wall-directed antibodies revealed precise spatiotemporal distributions of cell wall epitopes. An epidermal-like identity of early trichome walls matured into specialized wall domains over development. Cavity biogenesis was marked by separation of the subcuticular wall from the underlying surface wall in a homogalacturonan and α-1,5 arabinan epitope-rich zone and was associated with a reduction in fucosylated xyloglucan epitopes. As the cavity filled, a matrix with arabinogalactan and α-1,5 arabinan epitopes enclosed the metabolite droplets. At maturity, the disk cells' apical wall facing the storage cavity accumulated rhamnogalacturonan-I epitopes near the plasma membrane. Together, these data indicate that cannabis glandular trichomes undergo spatiotemporal remodeling at specific wall subdomains to facilitate storage cavity formation and metabolite storage.

Keywords: *Cannabis sativa* L. • Cell wall architecture • Electron microscopy • Fluorescence microscopy • Glandular trichomes • Glycome profiling

Editor-in-Chief's Choice

Introduction

Cannabis glandular trichomes produce an abundance of specialized metabolites, which are synthesized and secreted by a disk of cells into an extracellular storage cavity. As with many taxa (e.g. members of Solanaceae and Lamiaceae), cannabis glandular trichomes and their metabolites are associated with biotic or abiotic defense for the plant (Glas et al. 2012). Glandular trichome metabolites can act as a sticky trap for herbivorous insects (Simmons and Gurr 2005), a volatile cue to repel herbivores (Bleeker et al. 2009, 2011) or function directly as a toxic mixture (reviewed by Glas et al. 2012). The chemical properties of these metabolites can lead to toxicity to the plant itself, as has been shown for cannabis cells incubated with cannabigerolic acid and tetrahydrocannabinolic acid (Sirikantaramas et al. 2005). Autotoxicity of the glandular trichome disk cells is overcome by sequestration of the cannabinoids and terpenes in an extracellular storage cavity that develops on the glandular head (Livingston et al. 2020), which has led researchers to describe glandular trichomes as 'biofactories' because of their specialization for copious metabolite production (Huchelmann et al. 2017). As a result of selective breeding for highly productive strains of cannabis, the cannabinoid and terpenoid metabolites can represent up to 28% of the dry weight of the female flowers (Zager et al. 2019). Despite the importance of the cavity for metabolite storage and trichome function, very little is known about the composition of their cell walls, the mechanisms that lead to the cavity formation or how lipophilic metabolites are packaged in the hydrophilic apoplast.

The primary cell walls of flowering plants are generally composed of cellulose, hemicelluloses, pectins and glycoproteins. Cellulose is a linear chain of β(1,4)-linked glucose residues that interact with adjacent cellulosic chains to form ordered cellulose microfibrils, which in turn are the major load-bearing component of cell walls and afford cell wall tensile strength (reviewed in Cosgrove 2016, Anderson and Kieber 2020). Hemicelluloses are a group of biochemically diverse polysaccharides that display the capacity to cross-link within the cell wall, with xyloglucan being the predominant hemicellulose in eudicot primary cell walls (reviewed in Scheller and Ulvskov 2010). Pectins are complex polysaccharides classified into three groups: homogalacturonan (HG), rhamnogalacturonan-I (RG-I)

Downloaded from https://academic.oup.com/pcp/article/62/12/1944/6352475 by guest on 21 January 2025

Plant Cell Physiol. 62(12): 1944–1962 (2021) doi:https://doi.org/10.1093/pcp/pcab127, Advance Access publication on 2 September 2021, available online at https://academic.oup.com/pcp
© The Author(s) 2021. Published by Oxford University Press on behalf of Japanese Society of Plant Physiologists.
All rights reserved. For permissions, please e-mail: journals.permissions@oup.com

and rhamnogalacturonan-II (RG-II) (reviewed in Daher and Braybrook 2015). HG and RG-II are each composed of a galacturonic acid backbone. For HG, its properties are influenced by methyl groups attached to the carboxyl moiety, and removal of the methyl group by cell wall pectin methylesterases (PME) is a common wall modification (Willats et al. 2006, Wang et al. 2020). The RG-I backbone is composed of alternating rhamnose and galacturonic acid residues, which can be decorated with α-1,5 arabinans, galactans, and arabinogalactan side chains (reviewed in Mohnen 2008). The functions of pectic polysaccharides are dependent on numerous factors including species, cell type, and developmental stage. Pectins are generally considered to form the hydrated gel in which the cellulose–hemicellulose network is embedded (Bidhendi and Geitmann 2016). Lastly, primary cell walls also contain variable amounts of glycoproteins that may perform enzymatic or non-enzymatic functions with other cell wall polysaccharides. Arabinogalactan proteins (AGPs) are widely conserved members of the hydroxyproline-rich glycoprotein superfamily, a group of glycosylated proteins rich in arabinogalactan side chains (Johnson et al. 2017). The glycoprotein and polysaccharide constitution of the primary cell wall imparts control over cellular expansion, response to environmental stimuli and a myriad of cell-specific roles. The specific composition of cannabis glandular trichome cell walls remains unexplored but likely plays an important role in the accumulation of metabolites within the storage cavity (Schuurink and Tissier 2020).

Cannabis glandular trichomes are classified as having a subcuticular type of storage cavity, as the cavity forms via the separation of a cell wall layer directly below the cuticle, which increases in surface area and distends dramatically with metabolite accumulation in the apoplast (Tissier et al. 2017). In contrast to the hydrophilic primary cell wall, plant cuticles are lipidic. The cuticle consists of cutin, which is made of hydroxylated fatty acids covalently bound via polyester bonds, and hydrophobic waxes (Yeats and Rose 2013). This nonpolar layer forms the interface between the aerial epidermal cell wall and the external environment, functioning to reduce non-stomatal water loss and to protect the plant from UV light. Although the cell wall polysaccharides and cuticular fatty acids and waxes have distinct biosynthetic origins, chemical properties and functions in plant cells, the primary cell wall and cuticle do not have a clearly delineated boundary between them. The canonical representation of the cuticle has two distinct sub-structures: the cuticular layer, which represents a transition layer between cell wall polysaccharides, and the cuticle proper, which is primarily lipidic, with intra- and epicuticular waxes that surround and coat the cutin matrix (Jeffree 2006). In glandular trichomes with a subcuticular cavity, the chemical and physical properties of the cuticle, and the associated cell wall polysaccharides, must be important for the expansion and metabolite retention properties of the cavity (Tissier et al. 2017).

The formation of the cannabis subcuticular storage cavity proceeds via splitting of a specialized layer of the cell wall into two portions at the apical domain of the secretory cells, creating the apoplastic storage cavity (Hammond and Mahlberg 1978). Separation of this layer, called 'delamination', is thought to proceed via lysis of specific cell wall lamellae prone to degradation or remodeling. However, the composition of this specialized cell wall and the mechanisms that drive cell wall separation and expansion have not been investigated. Immunolabeling of tomato type VI glandular trichomes found HG and arabinan epitopes at the junction of the nascent intercellular storage cavity (Bergau et al. 2015), suggesting that pectin remodeling is involved in trichome cell–cell separation and cavity formation. Both cell–cell adhesion mediated by pectins in the middle lamella and numerous examples of pectin degradation/modification manifesting in cell–cell separation support this interpretation (Daher and Braybrook 2015).

The goal of this study was to reveal the spatiotemporal composition of cannabis glandular trichome cell walls from trichome initiation to metabolite storage within the subcuticular cavity. Glycome profiling and monosaccharide analysis were used to define the overall polysaccharide composition of cannabis glandular trichomes and to determine what polysaccharide groups are uniquely present or absent in these tissues compared to vegetative leaves, which are largely devoid of glandular trichomes. The glycomic analysis informed the selection of a panel of cell wall-directed antibodies that were used to perform extensive immunofluorescence and immunogold experiments to evaluate how the cell walls of cannabis glandular trichomes change during development. These data shed light on the process of cell wall remodeling, metabolite packaging within the cavity and prevention of metabolite leakage from the cavity.

Results

Morphological development of cannabis glandular trichome cavities

To reveal the cell wall ultrastructure of glandular trichomes at distinct stages of development, transmission electron microscopy (TEM) was used to image trichomes before, during and after storage cavity formation. Initial epidermal protuberances give rise to eight or more glandular cells arranged in a disk during the presecretory stage of development (Hammond and Mahlberg 1978, Livingston et al. 2020). Presecretory trichomes exhibited an apical cell wall domain that was contiguous with both the plasma membrane (PM) and cuticle across the tier of disk cells (**Fig. 1A**). The transition to early secretory stage of development was distinguished from presecretory trichomes by delamination of the apical disk cell wall (**Fig. 1B**). Cell wall delamination led to the formation of the storage cavity, which was bordered by the cell wall that remained associated with disk cells (defined as 'secretory disk surface wall') and the portion of wall that remained associated with the cuticle ('subcuticular wall domain'; **Fig. 1C**). Complete delamination across the tier of disk cells resulted in an extended cavity circumference, because of the production and secretion of an abundance of specialized metabolites from the underlying glandular trichome

Downloaded from https://academic.oup.com/pcp/article/62/12/1944/6352475 by guest on 21 January 2025

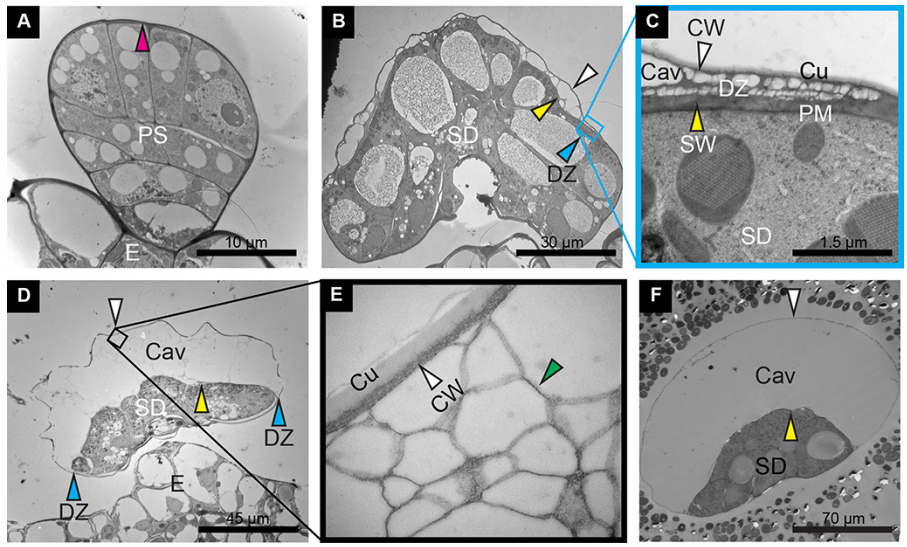

Fig. 1 Development of cannabis glandular trichome subcuticular storage cavities in cross-section. (A) Presecretory stage of trichome development. Apical wall (pink arrow) is contiguous with both the PM and cuticle. (B) Secretory trichome undergoing cavity formation at the delamination zone (cyan arrow), splitting into the secretory disk surface wall domain (yellow arrow) and the subcuticular wall domain (white arrow). (C) High magnification of box in (B) showing the ultrastructure of the delamination zone, which results in the formation of the secretory disk surface wall (yellow arrow) and the subcuticular wall (white arrow). (D) Mid-stage of cavity development showing expanded cavity containing numerous metabolite droplets within the cavity. (E) High magnification of box in (D) showing the ultrastructure of the intercompartmental cell walls (green arrow) beneath the subcuticular wall (white arrow). (F) Mature stage of cavity development showing large, distended cavity with few metabolite droplets. Yeast paste used as cryoprotectant for high-pressure freezing is seen surrounding the glandular trichome head. Cav: Cavity; Cu: Cuticle; CW: Subcuticular wall; DZ: Delamination zone; E: Epidermis; PS: Presecretory trichome; SD: Secretory disk cells; St: Stalk; SW: Secretory disk surface wall.

disk cells (**Fig. 1D**). As observed with two-photon microscopy (Livingston et al. 2020), these immature trichomes were filled with metabolites organized into numerous sub-compartments of various sizes delineated by intercompartmental wall fibrils (**Fig. 1E**). In more mature samples, the majority of floral trichomes had a multicellular stalk that raised the glandular head several hundreds of microns above the epidermal plane. Glandular trichomes that had reached this developmental stage had fully distended cavities and minimal sub-compartmentalization of metabolites (**Fig. 1F**). In summary, the TEM data provide an important context for the development of the cannabis trichome cell walls, highlighting three important cell wall-related phenomena: delamination of the apical cell wall giving rise to the nascent storage cavity, storage cavities at early stages of secretion contain metabolites organized into wall-delineated sub-compartments and, finally, the storage of large amounts of coalesced lipophilic metabolites within a hydrophilic cell wall cavity.

Glandular trichomes contain loosely bound xyloglucans and pectins

The composition of the cannabis glandular trichome cell walls has not been characterized; therefore, we investigated the polysaccharide composition of purified mature stalked glandular trichomes using glycomic profiling and monosaccharide analysis. To perform monosaccharide analysis on stalked glandular trichomes cell walls, metabolites were removed with sequential extractions of hexane, chloroform, ethanol and, finally, acetone, leaving only 10% of the original fresh tissue weight. The extracted dry tissue was then hydrolyzed with sulfuric acid, and the trichome monosaccharide profiles were determined. Glandular trichome wall extracts were primarily composed of galacturonic acid, xylose and glucose in relatively similar amounts and, to a lesser extent, galactose and arabinose (**Supplementary Table S1**). In comparison, the monosaccharide profile of vegetative leaves was dominated by glucose and, to a lesser extent, galacturonic acid and xylose (**Supplementary Table S1**). To understand how these constituent monosaccharides are arranged in the polysaccharides of glandular trichomes and leaves, alcohol-insoluble residues (AIR) were prepared from purified stalked glandular trichome heads and vegetative leaves that were harvested from mature cannabis plants. The AIR of both samples was subjected to sequential extraction in increasingly harsh treatments to extract cell wall components, followed by enzyme-linked immunosorbent assays (ELISA; Pattathil et al. 2012) with a panel of polysaccharide-directed monoclonal antibodies (Pattathil et al. 2010). The vegetative leaves served as a comparator tissue, and the results were largely consistent with glycomic analysis of other vegetative tissues, e.g. Arabidopsis leaves (**Fig. 2**; Pattathil et al. 2012). Overall, the types of cell wall polysaccharides detected in each sample were typical of primary cell wall samples. The sequential extraction of trichome cell wall components provides

Downloaded from https://academic.oup.com/pcp/article/62/12/1944/6352475 by guest on 21 January 2025

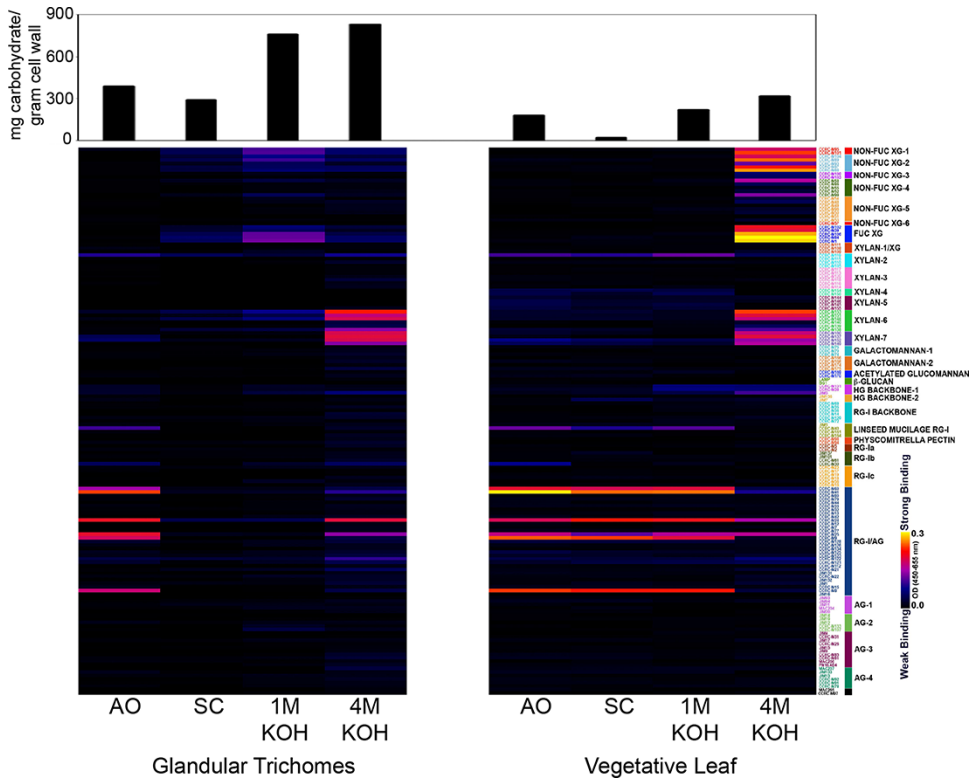

Fig. 2 Glycome profiles of isolated glandular trichomes and vegetative leaves from cannabis. ELISA-based glycome profiling using 155 glycan-directed monoclonal antibodies against cell wall AIR prepared from isolated glandular trichomes and whole vegetative leaves. Each column represents a sequentially extracted fraction of wall residue (AO: ammonium oxalate; SC: sodium carbonate; KOH: potassium hydroxide). Bars at the top indicate milligrams of carbohydrate extracted from 1 g of cell wall AIR of each fraction. Each cell represents binding intensity (scale in bottom right) for a single monoclonal antibody (represented as rows) for a particular sequential extract (represented in columns). Monoclonal antibodies are clustered based on the target polysaccharide group.

information about how tightly the epitopes, and by extension the cell wall polysaccharides, are bound within the cell wall structure. Pectic epitopes from vegetative leaves were predominantly detected in the ammonium oxalate, sodium carbonate and 1 M potassium hydroxide (KOH) extracts, with xyloglucans being released by 4 M KOH (**Fig. 2**). In contrast to the vegetative leaves, the glycome profile from cannabis trichomes showed ammonium oxalate alone was sufficient to extract glandular trichome pectic epitopes, with minimal epitope detection in the subsequent sodium carbonate and 1 M KOH extracts (**Fig. 2**). Similarly, fucosylated and non-fucosylated xyloglucans of glandular trichomes were readily extracted by 1 M KOH, in contrast to vegetative leaves, where 4 M KOH was necessary to release the same xyloglucan epitopes (**Fig. 2**). These data demonstrate that the xyloglucans and pectins are less tightly bound in glandular trichome cell walls relative to the cell walls of vegetative leaves.

Preliminary assessment of cell wall-directed antibodies in cannabis cross-sections

Based on the glycomic differences between mature glandular trichomes and vegetative leaves, a large panel of cell wall glycan- or protein-directed antibodies were screened for binding to cross-sections of 'Purple Kush' floral glandular trichomes from a range of different developmental stages (**Supplementary Table S2**). For each of the major groups of primary cell wall components, at least one antibody exhibited consistent and above-background fluorescence intensity in the glandular trichome tissues (**Supplementary Figs. S1–S3**) that were then used for comprehensive labeling across glandular trichome development. This approach allowed us to track the dynamic cell wall changes from early trichome initiation to the mature filled trichome.

Presecretory glandular trichome cell walls are unspecialized relative to underlying epidermal cells

As epidermis-derived tissues, we hypothesized that glandular trichomes at presecretory stages of development (**Fig. 1A**) have cell walls with similar composition to underlying epidermal cells. Cross-sections of cannabis flowers revealed immunoreactivity of HG-targeted antibodies in the calyx epidermis (**Fig. 3–D**). Methylesterified HG epitopes were abundantly detected with the LM20 antibody in the apical and basal domains of epidermis and presecretory trichomes, with scarce signal in the anticlinal

Downloaded from https://academic.oup.com/pcp/article/62/12/1944/6352475 by guest on 21 January 2025

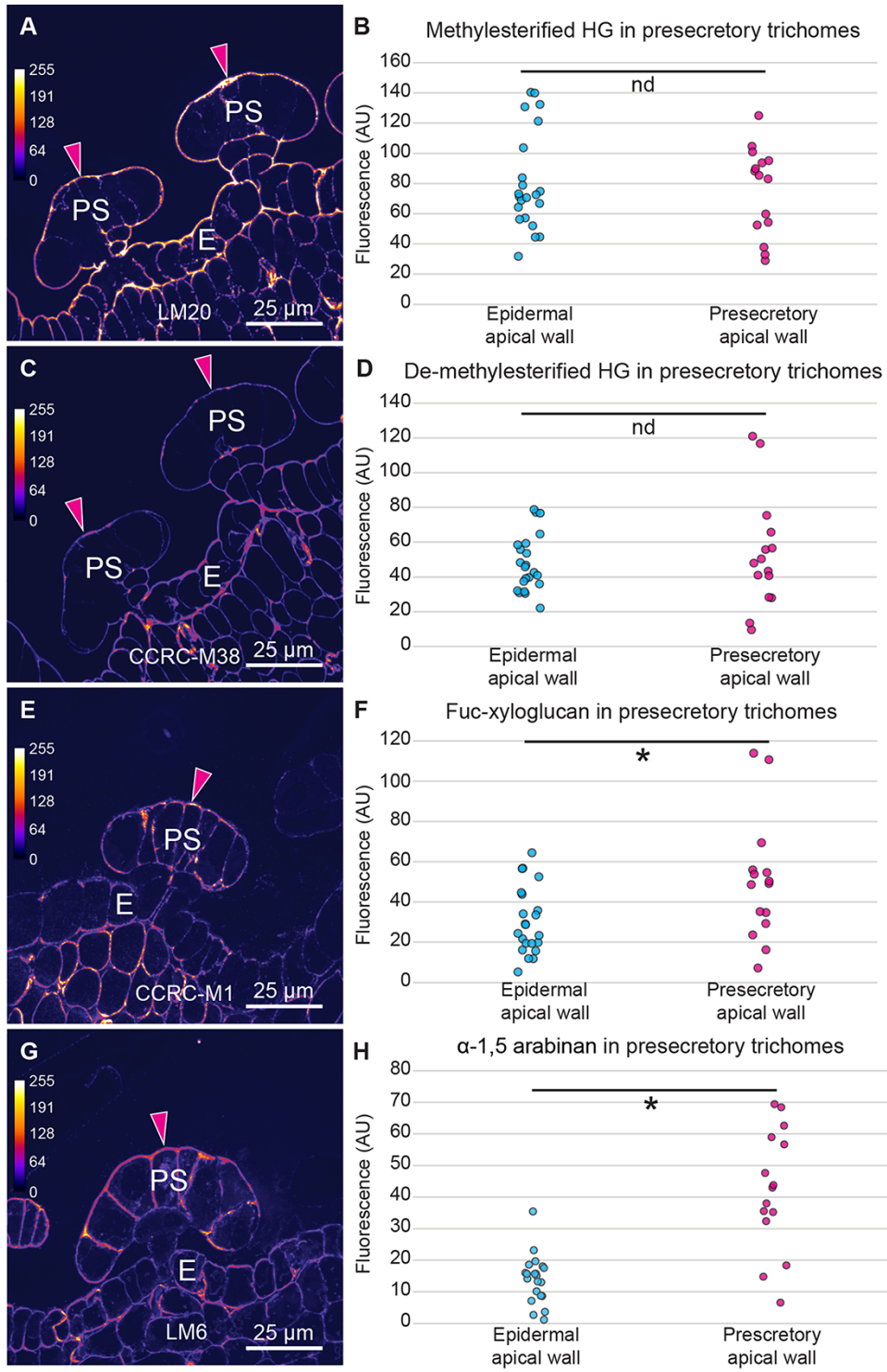

Fig. 3 Presecretory trichomes exhibit similar immunoreactivity to epidermal cell walls. Immunofluorescence analysis of (A-B) methylesterified homogalacturonan (HG), (C-D) de-methylesterified HG, (E-F) fucosylated xyloglucan and (G-H) α-1,5 arabinan epitopes in presecretory trichomes. (A, C, E, G) Immunofluorescent images of presecretory trichomes labeled with (A) LM20, (C) CCRC-M38, (E) CCRC-M1 and (G) LM6 antibodies. Antibody binding intensity is represented as a heat map (scale in top left). PS: Presecretory Trichome; E- Epidermis. Pink arrows indicate presecretory apical wall domain. (B, D, F, H) Quantification of (B) LM20, (D) CCRC-M38, (F) CCRC-M1 and (H) LM6 fluorescence intensity from the apical wall domains of epidermis ($n = 22$ biological replicates) and presecretory trichomes ($n = 15$ unique trichomes). Each dot represents the average fluorescence of all epidermal apical cell walls within an image or the average fluorescence of the apical domain of a unique trichome. Asterisks indicate statistically significant differences between groups according to Mann–Whitney U tests ($P < 0.05$).

Downloaded from https://academic.oup.com/pcp/article/62/12/1944/6352475 by guest on 21 January 2025

walls between adjacent cells of the trichomes (Fig. 3A, B). De-methylesterified HG epitopes were detected in a similar pattern using the CCRC-M38 antibody (Fig. 3C, D). In contrast, fucosylated xyloglucan epitopes were detected in all domains of the presecretory trichome head, as well as the epidermis, using the CCRC-M1 antibody (Fig. 3E, F). Fluorescence intensity in the apical domain of the presecretory gland head was higher than the epidermis (Fig. 3F). α-1,5 arabinan epitopes were abundantly detected in all domains of presecretory trichomes using the LM6 antibody, except the walls of stipe cells that connect the glandular disk to the underlying epidermis (Fig. 3G). α-1,5 arabinan labeling was significantly higher in presecretory trichomes compared to the epidermis (Fig. 3H). Together, these data indicate that presecretory glandular trichomes have similar cell walls to the calyx epidermis, especially in the components containing HG epitopes, although quantitative increases in α-1,5 arabinan and fucosylated xyloglucan epitopes emerged in the presecretory glandular trichome cell walls.

During delamination, trichomes have reduced fucosylated xyloglucans, HG modification and increased α-1,5 arabinans

The transition of presecretory glandular trichomes to the secretory stage is marked by the development of the subcuticular storage cavity on the glandular head. Based on the glycomic analysis that shows the presence of loosely bound fucosylated xyloglucans in glandular trichomes, we investigated whether fucosylated xyloglucan epitope density or spatial organization changes during the transition to the secretory stage of development. In contrast to the relatively homogenous and strong CCRC-M1 labeling of fucosylated xyloglucan epitopes in presecretory trichome walls (pink arrow in Fig. 4A), the CCRC-M1 label in all cell walls of the trichome was lower at the secretory phase, including the disk cell walls (yellow arrow in Fig. 4A). Quantification of these immunofluorescent signals supported an overall decrease in xyloglucan label as the trichome differentiated (Fig. 4B). The storage cavity and associated cuticle surrounding it were not labeled (Fig. 4A, white arrow), except low label at the site of delamination (Fig. 4A, blue arrow).

To observe the spatial distribution of fucosylated xyloglucan epitopes within the apical cell wall in that delamination zone, immunogold TEM labeling with CCRC-M1 and secondary antibodies tagged with gold particles was performed. The apical cell wall domain of presecretory trichomes contained gold particles throughout the wall (Fig. 4C), while secretory stage trichomes' delamination zones exhibited gold particles in the cell wall layer that remains adjacent to the PM (Fig. 4D). To illustrate the homogenous label of fucosylated xyloglucan epitopes across the presecretory apical walls compared to uneven distribution of epitopes in the secretory delamination zone and remaining disk cell wall, each gold particle's position within the apical wall was normalized to a range between 0 (PM) and 1 (cuticle) and then binned into deciles (Fig. 4E). Fucosylated xyloglucan epitopes in presecretory trichomes exhibited a largely normal distribution, with the majority of gold particles observed in the third and eight deciles of PM proximity (Fig. 4C, E). In contrast, the delamination zone of secretory trichomes exhibited a skewed distribution of epitopes, where gold particles were rarely observed in the lamellae undergoing delamination (Fig. 4D, E). Together, these data indicate that storage cavity biogenesis is associated with an overall reduction in fucosylated xyloglucan epitope labeling, and the same epitopes were largely absent from the actively delaminating wall layer.

The cannabis presecretory trichomes were rich in HG (Fig. 3), and de-methylesterification of HG has previously been implicated in the separation of intercellular walls during cavity formation in tomato type VI glandular trichome (Bergau et al. 2015). Therefore, the relationship between HG modification and cell wall delamination during subcuticular cavity formation in cannabis was examined. During the delamination stage, methylesterified and de-methylesterified HG label, recognized by the LM20 and CCRC-M38 antibody, respectively, was most intense in basolateral wall domains (Fig. 5A, B). With immunofluorescence, intensity in delamination zones was consistent with presecretory apical cell walls (Fig. 5C, D). For a high-resolution view of HG epitopes during delamination, immunoTEM was used to determine where HG epitopes were found within the apical cell wall (Fig. 5E–J). In presecretory trichomes, HG epitopes were detected in the distal half of the disk cells' apical cell wall, corresponding to the subcuticular layer. Gold particles corresponding to methylesterified HG, recognized by the LM20 antibody, were abundant in the regions of the wall where delamination was occurring, with lower levels in the wall layers proximal to the PM (Fig. 5F, G). This trend was more pronounced for de-methylesterified HG, recognized by the CCRC-M38 antibody, with enriched label in the subcuticular wall domain and minimal label in the secretory disk surface wall (Fig. 5I, J). Quantification of immunofluorescence label in the secretory disk surface wall also reflected a significant drop in the HG label following delamination (Fig. 5C, D). These data suggest that HG is an important component in cavity development, found directly in the layers of the cell wall where delamination occurs. The high-resolution mapping of both methylesterified and de-methylesterified HG illustrates how the apical cell wall is transformed during delamination, with the expansion and separation of the subcuticular wall leaving behind a secretory disk surface wall with low HG levels.

As the anti-α-1,5 arabinan LM6 antibody prominently labeled presecretory trichomes, we examined its distribution during delamination. While LM6 binding was found in all cell wall domains surrounding the secretory disk cells (Fig. 6A), the fluorescence intensity was highest in zones of active delamination (Fig. 6B). This reflects either an increase in epitope abundance or, as a result of delamination, the α-1,5 arabinan

Downloaded from https://academic.oup.com/pcp/article/62/12/1944/6352475 by guest on 21 January 2025

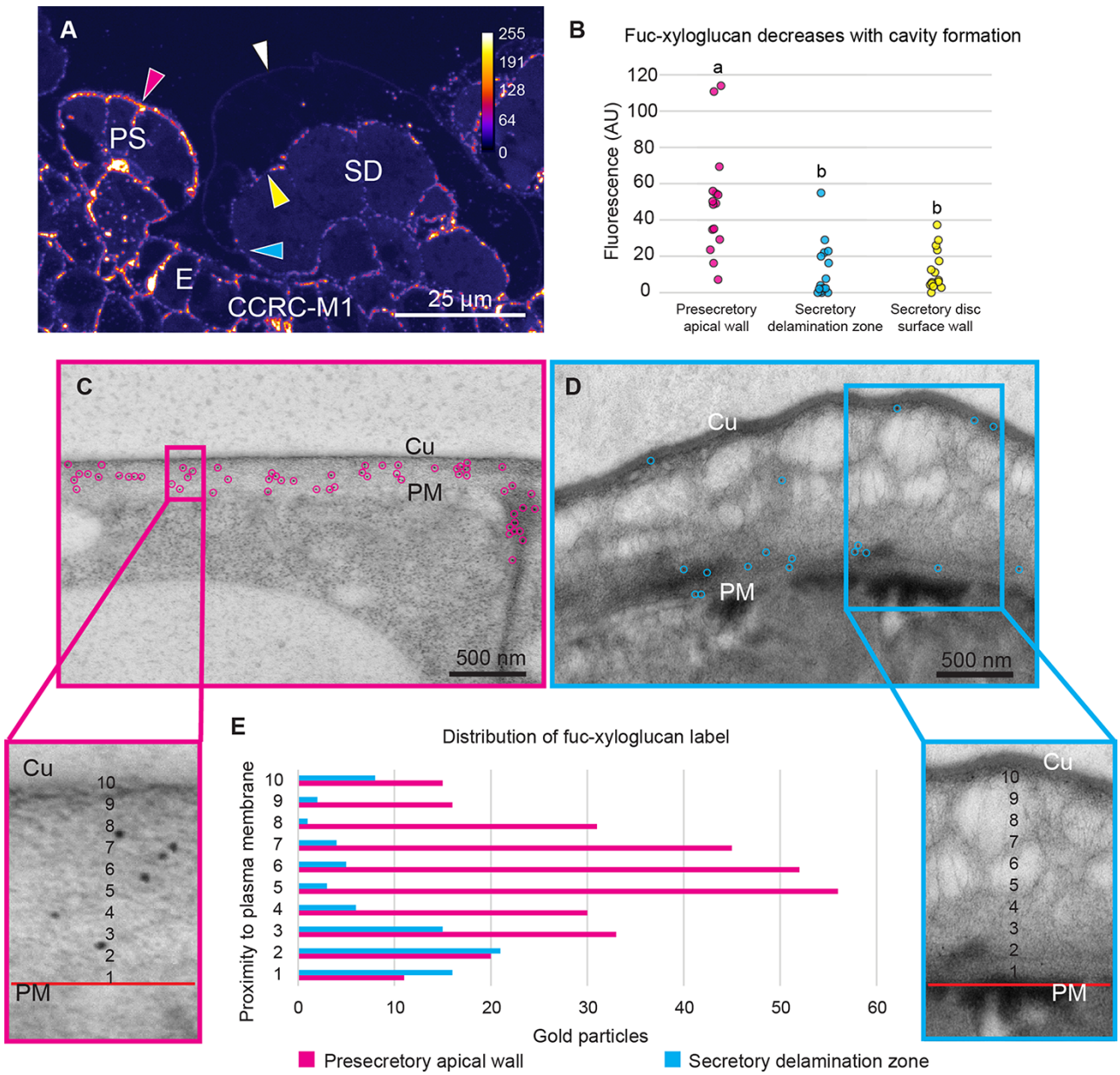

Fig. 4 Fucosylated xyloglucan labeling decreases with cavity formation. (A) Immunofluorescent image of presecretory and early secretory glandular trichomes labeled with CCRC-M1. Antibody binding intensity represented as a heat map (scale in top right corner). PS: Presecretory trichome; SD: Secretory disk; E: Epidermis. Pink arrowhead indicates presecretory apical wall; cyan arrowhead indicates secretory delamination zone; yellow arrowhead indicates secretory disk surface wall; white arrowhead indicates subcuticular wall. (B) Quantification of immunofluorescence intensity of CCRC-M1 in each wall domain ($n = 15$ unique trichomes for each group). Each dot represents the average fluorescence of a unique trichome's wall domain. Letters indicate statistically significant differences between groups ($P < 0.05$) determined by post-hoc pair-wise comparisons with Dunn's procedure with a Bonferroni correction for multiple comparisons. (C-D) ImmunoTEM labeling of the CCRC-M1 antibody in the (C) presecretory apical wall and (D) secretory delamination zone. Insets show method of quantifying gold particle proximity to PM. Pink and cyan circles indicate gold particles in (C) and (D), respectively. Walls of variable thickness were divided into deciles corresponding to distance from the PM to the cuticle. Red line indicates the PM. (E) Distribution of immunoTEM gold particles in deciles of each wall domain as a function of proximity to the PM ($n = 3$ unique trichomes for each trichome group).

backbone becomes more exposed. ImmunoTEM labeling with LM6 showed an abundance of gold particles in secretory stage trichomes in the lamellae undergoing active delamination (**Fig. 6D**). These data show that the secretory delamination zone is rich in α-1,5 arabinan-containing polysaccharides, which could include RG-I and/or AGPs.

Downloaded from https://academic.oup.com/pcp/article/62/12/1944/6352475 by guest on 21 January 2025

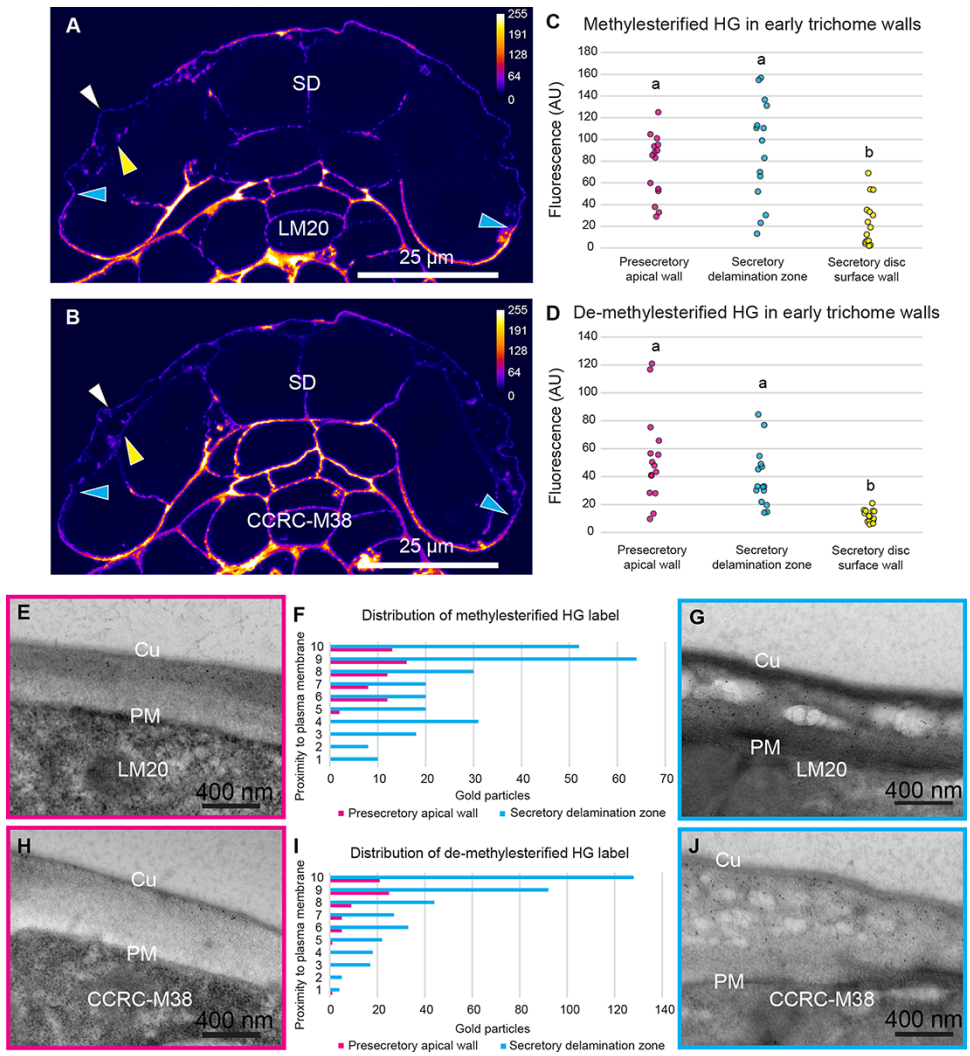

Fig. 5 Homogalacturonan-rich subcuticular wall domain is the site of wall delamination. (A-B) Equivalent sections of a glandular trichome during early cavity formation immunolabeled with (A) LM20 and (B) CCRC-M38. Antibody binding intensity represented as a heat map (scale in top right corner). SD: secretory disk. Cyan arrowhead indicates delamination zone; yellow arrowhead indicates secretory disk cell wall; white arrowhead indicates subcuticular wall. (C-D) Quantification of immunofluorescence intensity for (C) LM20 and (D) CCRC-M38 presecretory apical walls, secretory delamination zones and secretory disk surface wall ($n = 15$ unique trichomes for each group). Each dot represents the average fluorescence of a unique trichome's wall domain. Letters indicate statistically significant differences between groups ($P < 0.05$) determined by post-hoc pair-wise comparisons with Dunn's procedure with a Bonferroni correction for multiple comparisons. (E-J) ImmunoTEM localization of LM20 and CCRC-M38 antibodies. (E, H) ImmunoTEM images of presecretory trichome apical wall domain. (G, J) ImmunoTEM images of secretory delamination zone. (F, I) Distribution of gold particles in presecretory apical walls ($n = 3$ unique trichomes for each antibody) and secretory delamination zones ($n = 3$ unique trichomes for each antibody). Walls of variable thickness were divided into deciles corresponding to distance from the PM to the cuticle (see **Fig. 4** for visual description). Cu: cuticle.

Metabolite droplets are delineated by α-1,5 arabinan and arabinogalactan epitopes in the storage cavity

Progression of the secretory stage of trichome development results in complete delamination of the apical cell wall. Trichomes at this stage contain an enlarged cavity with highly compartmentalized metabolite droplets (Livingston et al. 2020). Neither fucosylated xyloglucan nor HG epitopes were detected in the intercompartmental walls of the storage cavity (**Supplementary Fig. S4**). In contrast, α-1,5 arabinan and arabinogalactan-containing glycoproteins were associated with metabolite compartmentalization within the storage cavity (**Fig. 7**). LM6 labeling of α-1,5 arabinan epitopes was detected throughout the storage cavity, including the intercompartmental walls between cavity droplets (**Fig. 7A**). AGPs labeled with JIM13 were detected abundantly in intercompartmental wall domains, with relatively weak labeling in the secretory disk surface wall (**Fig. 7B**). Interestingly, the

Downloaded from https://academic.oup.com/pcp/article/62/12/1944/6352475 by guest on 21 January 2025

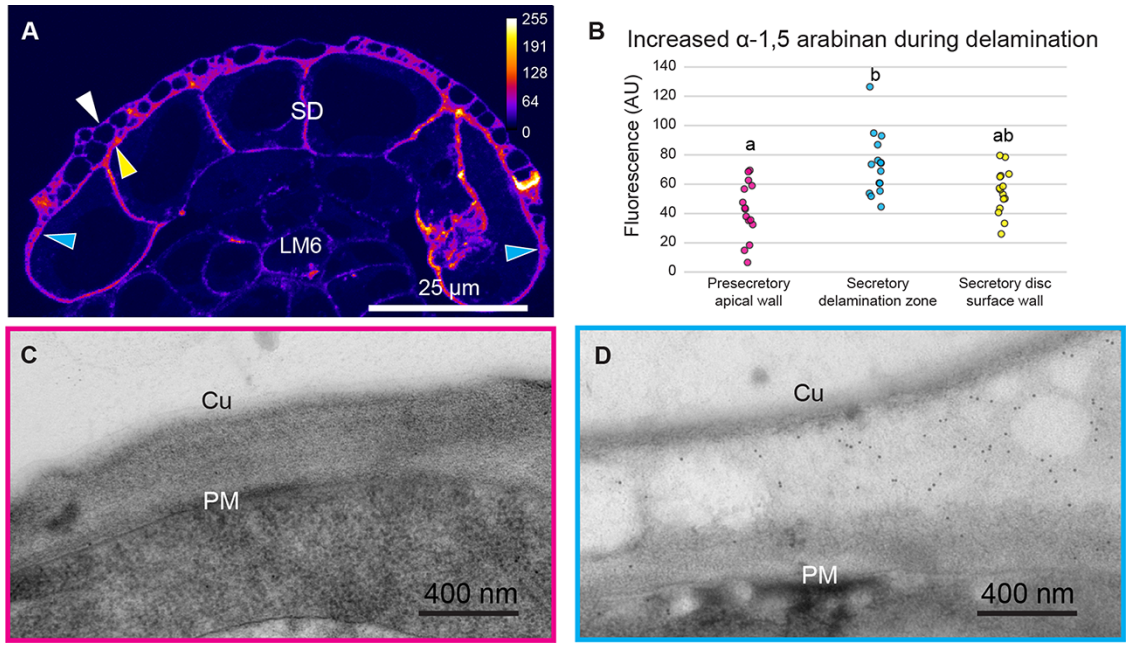

Fig. 6 Delamination is associated with increased α-1,5 arabinan epitopes. (A) Immunofluorescent labeling of a glandular trichome during early cavity formation with LM6 antibody. Antibody binding intensity represented as a heat map (scale in top right corner). Cyan arrowhead indicates secretory delamination zone; yellow arrowhead indicates secretory disk surface wall; white arrowhead indicates subcuticular wall. SD: secretory disk. (B) Quantification of LM6 fluorescence in glandular trichome presecretory apical walls, secretory delamination zones and secretory disk surface walls ($n = 15$ unique trichomes for each group). Each dot represents the average fluorescence of an individual trichome. Letters indicate statistically significant differences between groups ($P < 0.05$) determined by post-hoc pair-wise comparisons with Dunn's procedure with a Bonferroni correction for multiple comparisons. (C-D) ImmunoTEM labeling of the (C) presecretory apical domain and (D) secretory delamination zone labeled with LM6 (representative images from three unique trichomes of each trichome stage). Cu: cuticle.

arabinogalactan-containing glycoprotein epitope detected by the LM1 antibody was restricted to the intercompartmental wall domains within the cavity with no detectable fluorescence in any other glandular trichome wall domain (**Fig. 7C**). This pattern of labeling was unexpected, as these epitopes were neither detected at any previous stage of development nor in the disk cell surface wall domains of secretory stage trichomes. ImmunoTEM using LM6, JIM13 and LM1 antibodies revealed the nanoscale distribution of these epitopes in the intercompartmental boundaries between droplets (**Fig. 7D–F**). These data define the boundary surrounding metabolite droplets in secretory glandular trichome cavities as a glycoprotein-rich cell wall domain containing α-1,5 arabinan and arabinogalactan-containing glycoproteins.

During stalked trichome maturation, the metabolite droplets coalesce into a single large droplet (Livingston et al. 2020) and, as a result, the intercompartmental walls are lost. We hypothesized the remodeling events that occur due to coalescence would result in displacement of α-1,5 arabinan and arabinogalactan-containing glycoprotein epitopes to the subcuticular wall and disk surface wall. This hypothesis was supported by α-1,5 arabinan epitope labels, which were abundantly detected by LM6 in the residual intercompartmental wall domains, the subcuticular wall and secretory disk surface wall (**Fig. 7G, J**). In contrast, glycoprotein epitopes exhibited low antibody binding intensity surrounding the large resin droplet. AGP detection with JIM13 was significantly lower in both the disk cell surface and subcuticular wall domains compared to intercompartmental wall domains (**Fig. 7K**). Surprisingly, the epitopes detected by LM1 were absent from all domains of stalked glandular trichome cavities (**Fig. 7L**). LM1 labeling was only detected in the abscission cells subtending the glandular trichome head (**Fig. 7I**). These data indicate that mature cavities have abundant α-1,5 arabinan epitopes in the cavity periphery; however, the glycoprotein epitopes delineating the metabolite droplets in early trichomes are lost during cavity maturation.

Cuticle thickness increases, while secretory disk cell wall is maintained, following cavity development

We have shown that glandular trichomes undergo significant reduction in cell wall epitope detection of fucosylated xyloglucans (**Fig. 4**), HGs (**Fig. 5**) and arabinogalactans (**Fig. 7**) as trichomes progress from the presecretory stage to mature stalked trichomes. Therefore, we hypothesized that the thickness of secretory trichome walls is reduced compared to that of presecretory trichome walls. We used TEM to evaluate the thickness of presecretory apical walls (**Fig. 8A**) compared to that of the secretory cell walls that are derived from it: the secretory

Downloaded from https://academic.oup.com/pcp/article/62/12/1944/6352475 by guest on 21 January 2025

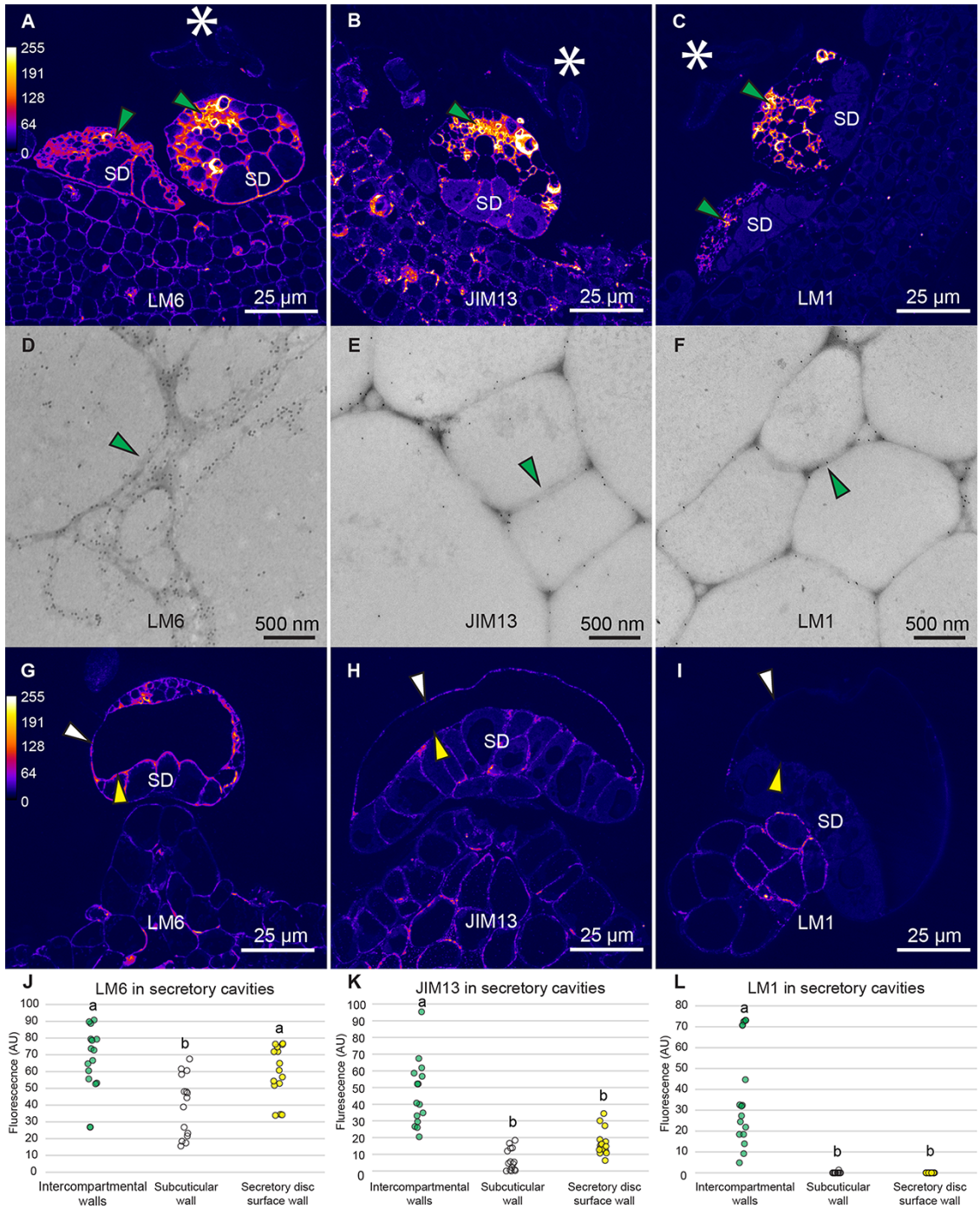

Fig. 7 Intercompartmental walls are delineated by α-1,5 arabinan and glycoprotein epitopes. (A-C) Equivalent Immunofluorescent images of compartmentalized glandular trichome cavities labeled with (A) LM6, (B) JIM13 and (C) LM1 antibodies. Antibody binding intensity is represented as a heat map (scale in top left of A). (D-F) ImmunoTEM images of intercompartmental wall domains in compartmentalized glandular trichome cavities labeled with (D) LM6, (E) JIM13 and (F) LM1 antibodies (representative images from three unique trichomes for each antibody). (G-I) Immunofluorescent images of mature stalked glandular trichomes labeled with (G) LM6, (H) JIM13 and (I) LM1 antibodies. Antibody binding intensity is represented as a heat map (scale in top left of G). (J-L) Quantification of (J) LM6, (K) JIM13 and (L) LM1 fluorescence in glandular trichome intercompartmental walls, subcuticular walls and secretory disk surface walls ($n = 15$ unique trichomes for group). Each dot represents the average fluorescence of an individual trichome. Letters indicate statistically significant differences between groups ($P < 0.05$) determined by post-hoc pair-wise comparisons with Dunn's procedure with a Bonferroni correction for multiple comparisons. Green arrows and dots indicate intercompartmental walls, white arrows and dots indicate subcuticular walls, yellow arrows and dots indicate secretory disk surface wall. SD indicates glandular trichome secretory disk. White asterisk indicates set of non-glandular trichomes in cross-section.

Downloaded from https://academic.oup.com/pcp/article/62/12/1944/6352475 by guest on 21 January 2025

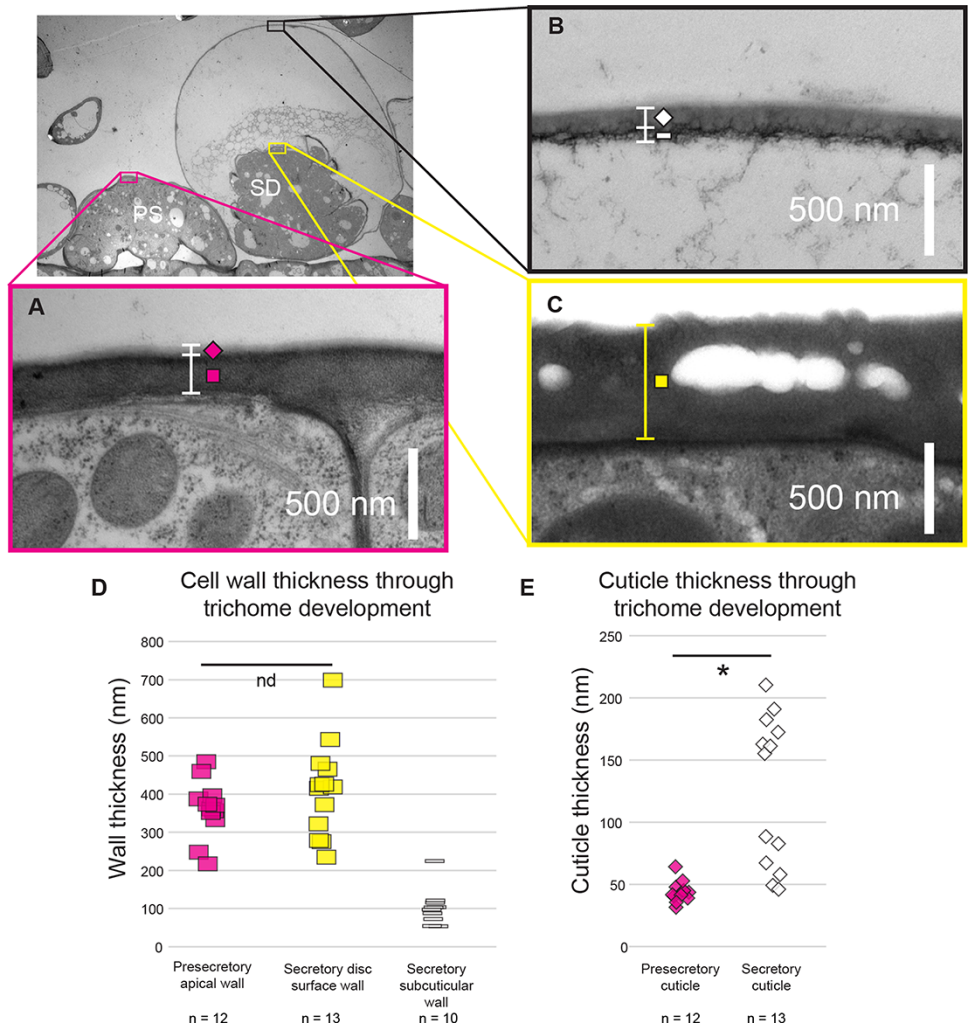

Fig. 8 Cell wall and cuticle thickness does not decrease with cavity development. (A–C) TEM micrographs of the (A) presecretory apical wall, (B) the cuticular sheath of a secretory trichome and (C) the secretory disk surface wall. Measurements indicated with squares correspond to the presecretory/secretory surface measurements, diamonds correspond to cuticle measurements and horizontal lines correspond to the secretory subcuticular wall. PS: presecretory trichome; SD: secretory disk. (D–E) Quantification of (D) cell wall and (E) cuticle thickness measurements. Pink symbols correspond to presecretory apical domain measurements; yellow symbols correspond to secretory disk surface wall measurements; white symbols indicate subcuticular wall or cuticle measurements. Each symbol represents the average of five measurements for a unique trichome. Asterisks indicate statistically significant differences between groups according to Mann–Whitney U tests ($P < 0.05$).

subcuticular wall (**Fig. 8B**) and the secretory disk surface wall (**Fig. 8C**). The thickness of the secretory disk surface wall alone was not significantly different from the presecretory apical wall (**Fig. 8D**), suggesting that the cell wall surrounding the secretory disk cells is maintained despite the dynamic fluctuations in cell wall components during storage cavity formation. In contrast, the cuticle of secretory trichomes was significantly larger than the cuticles of presecretory trichomes (**Fig. 8E**). These data show that delamination from the presecretory apical wall and substantial expansion of the cavity as a whole is accompanied by continued deposition of cuticular lipids and possibly cell wall polysaccharides.

RG-I epitopes accumulate in secretory trichome disk cell walls

Secretory stage glandular trichomes may modify their cell walls in a way that retains the hydrophobic metabolites within the apoplast to reduce release of volatile organic compounds and exudation of resin out of the cavity either through the cuticle or backflow into the disk cell cytosol. One potential route of reinforcing the cavity may be achieved by secreting additional wall components as the cavity matures. Therefore, we hypothesized that cell wall components not previously detected in early stages of trichome development may emerge in the disk surface wall during maturation. Interestingly, RG-I epitopes were

Downloaded from https://academic.oup.com/pcp/article/62/12/1944/6352475 by guest on 21 January 2025

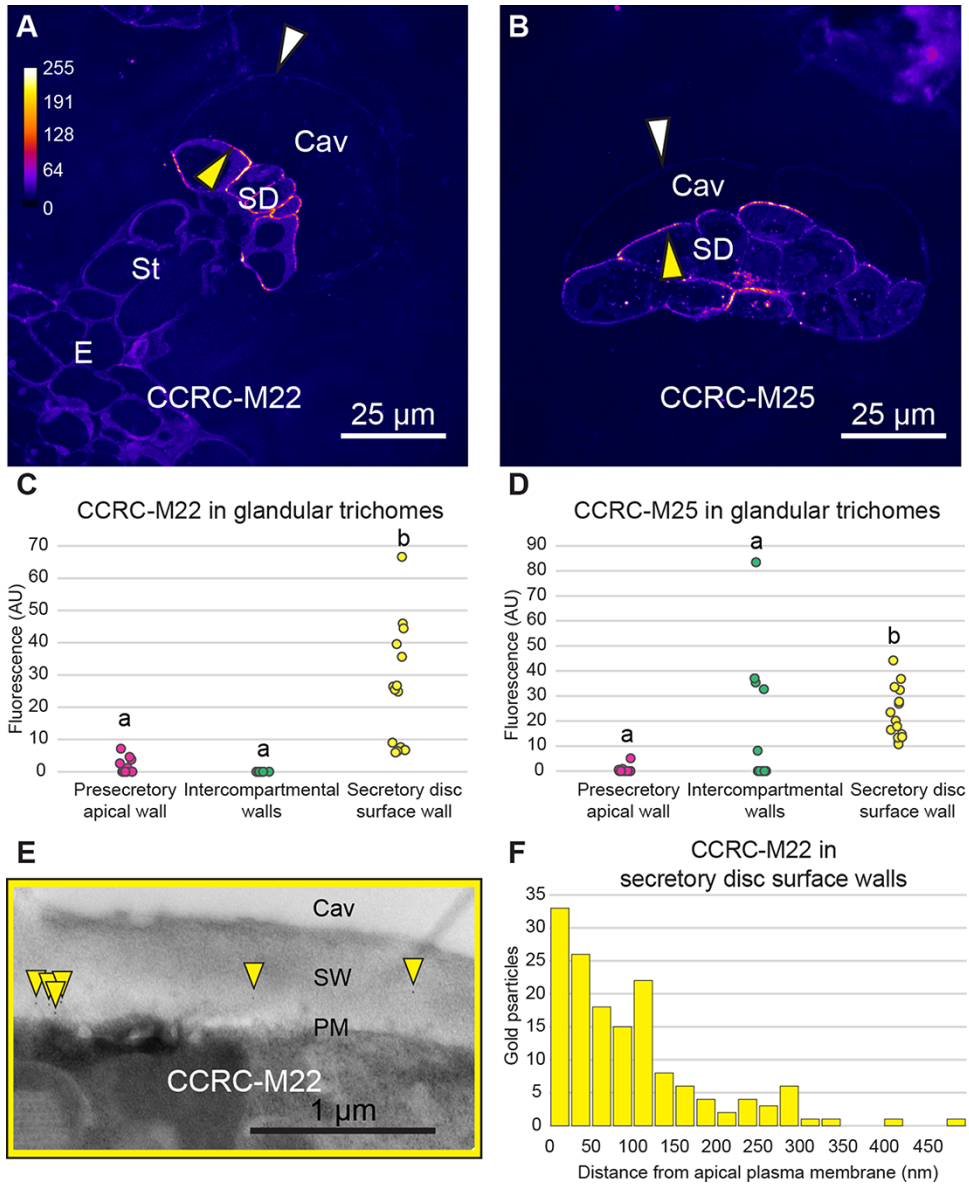

Fig. 9 RG-I epitopes emerge in secretory disk cell walls during cavity maturation. (A-B) Immunofluorescent images of stalked mature glandular trichomes labeled with (A) CCRC-M22 and (B) CCRC-M25 antibodies. Antibody binding intensity is represented as a heat map (scale in top left corner of A). Yellow arrowhead indicates secretory disk surface wall; white arrowhead indicates subcuticular wall. Cav: Cavity; E: Epidermis; SD: secretory disk; St: stalk. (C-D) Quantification of immunofluorescence intensity for (C) CCRC-M22 and (D) CCRC-M25 glandular trichome wall domains ($n = 15$ unique trichomes for each group). Each dot represents the average fluorescence of an individual trichome's wall domain letters indicate statistically significant differences between groups ($P < 0.05$) determined by post-hoc pair-wise comparisons with Dunn's procedure with a Bonferroni correction for multiple comparisons. (E) ImmunoTEM labeling of the CCRC-M22 antibody in the secretory disk surface wall of glandular trichomes. Yellow arrowheads indicate the position of gold particles. Cav: Cavity; SW: Secretory disk surface wall. (F) Distribution of CCRC-M22 gold particles in the secretory disk surface wall as a function of distance from PM ($n = 6$ unique trichomes; at least three images from each trichome were used for quantification).

detected in secretory stage disk cell walls with CCRC-M22 and CCRC-M25 (**Fig. 9A, B**). In the case of CCRC-M22, label was detected exclusively within the secretory disk walls but not in the intercompartmental wall domains of pre-stalked cavities or in presecretory trichomes (**Fig. 9C**). CCRC-M25 label was found consistently in secretory disk walls and, inconsistently, in the intercompartmental walls of pre-stalked trichomes (**Fig. 9D**). Immuno-TEM using CCRC-M22 revealed an enrichment of gold particles in close proximity to the apical PM within the secretory disk surface wall (**Fig. 9E**), with 80% of all gold particles observed within 150 nm of the apical PM (**Fig. 9F**). These data suggest that RG-I epitopes in secretory disk surface walls

Downloaded from https://academic.oup.com/pcp/article/62/12/1944/6352475 by guest on 21 January 2025

are deposited in close proximity to the PM during cavity maturation.

Discussion

Understanding the wall components and mechanisms involved in the formation of glandular trichome storage cavities has been largely uninvestigated across plant species. In this study, we correlated the development of the metabolite-filled subcuticular cavity of cannabis glandular trichomes cell walls (**Fig. 1**) with dynamic spatiotemporal modifications in their cell walls. Monosaccharide analysis of purified glandular trichome walls revealed an enrichment of xylose- and galacturonic acid-containing polysaccharides compared to vegetative leaves (**Supplementary Table S1**), while glycome profiling indicates that pectic and xyloglucan epitopes are more easily extracted from trichome cell walls compared to leaf cell walls (**Fig. 2**). Three important developmental events occur during subcuticular cavity formation and metabolite filling in cannabis. First, the cell wall delaminates along the apical surface of the secretory disk cells. While in early stages of trichome development the cell walls are similar to underlying epidermis (**Fig. 3**), delamination of the storage cavity is associated with loss or modification of fucosylated xyloglucans (**Fig. 4**). The presence of pectin during delamination was apparent from labeling with antibodies against both high methylesterified HG and non-methylesterified HG. These pectins were initially restricted to the subcuticular layer, became abundant in the delamination zone and declined in the cell wall covering the disk cells as the cavity matured (**Fig. 5**). The second important developmental milestone is early metabolite accumulation in an emulsion-like compartmentalized cavity. As shown in **Figs. 6**, **7**, metabolites within the cavity are encapsulated by glycoprotein and α-1,5 arabinan-rich RG-I. Third, maturation of the storage cavity, where metabolites coalesce into a large central droplet, was associated with loss of glycoprotein epitope detection. At maturity, the wall covering the secretory disk facing the storage cavity had a specific subset of RG-I epitopes coating the cells' surfaces (**Fig. 9**). The value of using cell wall-directed antibodies at the nanoscale level is illustrated as many of these modifications were specific to layers or subdomains of cell walls, indicating precise control of cell wall remodeling during trichome development.

In cannabis glandular trichomes, fucosylated xyloglucan detection was reduced in the cell wall lamellae undergoing delamination. The role of xyloglucans in primary cell wall growth and expansion is enigmatic and remains a major field of study (Cosgrove 2016, 2018). Xyloglucans interact with cellulose microfibrils, potentially contributing to or modifying microfibril-microfibril biomechanical 'hot spots' (Zhang et al. 2016). During growth, xyloglucan-cellulose microfibril interactions can be modified within the wall by a suite of different wall enzymes, including xyloglucan endotransglucosylase-hydrolases (XTH) to facilitate wall creep, although there are few reports of its involvement in lysis and separation of cell wall lamellae. XTHs may contribute to fruit ripening (Witasari et al. 2019), which involves modification to cell wall ultrastructure and cell–cell separation (Prasanna et al. 2007). Three XTHs are in the top 1,000 highly expressed transcripts of cannabis glandular trichomes (i.e. PK09372, PK03350 and PK02654; Livingston et al. 2020), which have not been functionally characterized. With xyloglucans more easily extracted from cannabis glandular trichomes compared to cannabis leaves (**Fig. 2**), as well as a substantial reduction in fucosylated xyloglucan labeling in all domains of secretory trichomes compared to presecretory trichomes, our data indicate that the modification and potential degradation of fucosylated xyloglucans accompanies cell wall delamination as the storage cavity forms.

During early cavity formation, methylesterified and de-methylesterified HG epitopes were both found abundantly in active delamination zones. These epitopes decreased significantly once the subcuticular wall had separated entirely from the apical wall (**Fig. 5**). HG and its modification/degradation is involved in numerous examples of modulating cell wall adhesion separation (Daher and Braybrook 2015). While HG is secreted in a highly methylesterified state, de-methylestereriffication by PME can promote HG degradation by polygalacturonase enzymes, for example, in pollen tetrad separation (Francis et al. 2006, Ogawa et al. 2009), fruit ripening (Wang et al. 2019) and fruit abscission (Merelo et al. 2017). In tomato glandular trichomes, cavity formation has been associated with the presence of de-methylesterified HG in the walls surrounding the cavity (Bergau et al. 2015). While there are no annotated HG modifying proteins in the top 1,000 most highly expressed transcripts in glandular trichomes (Livingston et al. 2020), one of the top 10 transcripts corresponds to a BURP-domain containing protein (PK18932). BURP domains are found in a diverse set of proteins, of which several are associated with modification or relaxation of the cell wall. For example, a BURP-domain-containing non-catalytic subunit of polygalacturonase (PG1β) from tomato is thought to interact with cell wall polysaccharides and the catalytic subunit of polygalacturonase to regulate the metabolic activity of polygalacturonase (Zheng et al. 1992, 1994). In addition, the BURP-domain-containing PGL3 from *Arabidopsis thaliana* regulates cell wall expansion in concert with cell wall-localized expansins (Park et al. 2015). The enzymes responsible for the HG breakdown in cannabis trichomes have not been identified, so a potential role for the cannabis BURP-domain-containing proteins remains speculative.

The abundance of α-1,5 arabinan detected within the delamination zone, secretory disk surface wall and subcuticular wall domains indicates that α-1,5 arabinan-rich RG-I or AGPs or both are important components of cavity formation. The presence of LM6 in trichome walls undergoing delamination is consistent with reports of these epitopes in a wide variety of tissues involved in cell–cell separation. Sloughing of root cap cells (Willats et al. 1999), citrus fruit ripening (Merelo et al. 2017) and somatic embryogenesis in *Quercus suber* (Pérez-Pérez et al. 2019) exhibit an increase in LM6 labeling following cell–cell separation in each system. In particular, the appearance of

Downloaded from https://academic.oup.com/pcp/article/62/12/1944/6352475 by guest on 21 January 2025

LM6 epitopes was reported in tomato glandular trichome cell walls after storage cavity formation (Bergau et al. 2015). The functional role of α-1,5 arabinans in cell–cell separation is not known, but they have been shown to promote flexibility in the walls of guard cells, which undergo reversible wall deformation during stomatal opening and closure (Jones et al. 2003). α-1,5 arabinans detected throughout glandular trichome development may be important in facilitating distension and flexibility of the intercompartmental and subcuticular walls.

Previously, we have shown that the cannabinoids and terpenes in sessile and pre-stalked glandular trichomes accumulate in numerous droplets within the storage cavity (Livingston et al. 2020). Our data in this study provide evidence that the droplets are separated by a unique intercompartmental cell wall domain containing arabinogalactan-containing glycoproteins and α-1,5 arabinan-containing polysaccharides (**Fig. 7**). Coalescence or loss of these intercompartmental walls during cavity maturation is associated with a loss of glycoprotein epitopes (**Fig. 8**), which suggests that the metabolite droplets may be transiently stabilized within the cavity by arabinogalactan-containing glycoproteins. These extracellular droplets are distinct from intracellular oil bodies, such as the intracellular lipid globules of liverworts containing a variety of terpenoids packaged in a proteinaceous matrix of unknown composition (He et al. 2013). Similarly, intracellular compartmentalization of triacylglycerol storage lipids relies on half-unit membranes composed of lipids and proteins (e.g. oleosins) that bud from the endoplasmic reticulum in seed plants (reviewed by Pyc et al. 2017) and moss (Huang et al. 2009). Our ultrastructural data neither show evidence of an analogous lipid droplet-like mechanism occurring at the PM nor a membrane delimitation at the periphery of the cavity compartments.

The arrangement of droplets within cannabis glandular trichome storage cavities represents an oil-in-water emulsion, where the lipidic cannabinoid and terpene metabolites are surrounded by hydrophilic apoplast. Polysaccharides and proteins are frequently used in the food industry as emulsifiers or stabilizers of emulsification. Two of the major naturally occurring emulsification agents in the food industry are gum arabic and sugar beet pectin, both of which are complex mixtures of polysaccharides and glycoproteins. Gum arabic consists of ∼90% arabinogalactan polysaccharides and ∼10% AGPs (Williams et al. 2000), while sugar beet pectin is composed of α-1,5 arabinan-containing RG-I and HG (Morris et al. 2010), as well as arabinogalactan-containing glycoproteins (Nuñez et al. 2009). Interestingly, the JIM13 and LM1 antibodies show strong cross-reactivity with both gum arabic (Yates et al. 1996, Pattathil et al. 2010) and arabinans from sugar beet pectins (WallMabDB), while LM6 has strong cross-reactivity with sugar beet pectin (Willats et al. 1998) and arabinan domains in some AGP sidechains (Verhertbruggen et al. 2009). A review of the literature by Evans et al. (2013) led the authors to argue that the amphiphilic properties of gum arabic and sugar beet proteins confer the interfacial properties required for emulsifying lipidic compounds in a polysaccharide gel. Given that sugar beet pectin and gum arabic are effective emulsifying agents of limonene (Siew and Williams 2008, Padala et al. 2009) and medium-chain triglycerides (Funami et al. 2007), the detection of JIM13, LM1 and LM6 antibody binding in the intercompartmental domains of developing cannabis cavities supports the interpretation that cannabinoid and terpene droplets are stabilized into an emulsion by arabino(galactan)-containing glycoproteins and polysaccharides.

JIM13 and LM1 labels for arabinogalactan-containing glycoproteins do not emerge until after cavity biogenesis (**Fig. 7**). Although the emergence of their epitopes coincide developmentally, the LM1 antibody label is exclusively restricted to intercompartmental walls, while JIM13 is also present at the apical and anticlinal wall domains of the disk cells. The glycoproteins detected by JIM13 may be secreted from the disk cells at the same time as metabolite secretion. If AGPs are produced and secreted at the same time as the cannabinoid/terpene metabolites, they could interact with metabolites at the secretory disk surface wall and form the emulsions required for cannabinoid partitioning into the hydrophilic cell wall. The apparent loss of glycoprotein epitopes in mature stalked glandular trichome cavities is puzzling. Coalescence of the metabolite droplets would displace the glycoprotein-rich intercompartmental walls to the periphery of the cavity; however, the arabinogalactan-containing glycoproteins detected with LM1 and JIM13 were not seen in the periphery of the mature stalked trichome cavity (**Fig. 7**). The simplest explanation for these observations is degradation of the antibody epitopes *in muro*. Transcriptomic data from isolated glandular trichomes demonstrated abundant carbohydrate-active enzymes that could be responsible (Livingston et al. 2020), although their functional roles in cannabis trichomes awaits experimental testing.

The final stages of glandular trichome cavity development are marked by the coalescence of metabolite droplets into fewer, larger droplets (Livingston et al. 2020). In this study, RG-I epitopes emerged at the secretory disk surface wall domain of glandular trichomes nearing maturity, as detected with CCRC-M22 and CCRC-M25 (**Fig. 9**). The heterogenous structure of RG-I is reflected in a variety of complex and poorly understood physiological roles in plant cell walls, although it is generally considered to be involved in modulating wall extensibility and firmness (Bidhendi and Geitmann 2016). RG-I gelation by galactan-rich RG-I can impart more dense gel formation and reduced compression compared to arabinan-rich RG-I (Mikshina et al. 2015). Similarly, RG-I with depleted arabinan exhibited greater stiffening in stomatal cells compared to untreated controls (Jones et al. 2003). The CCRC-M22 and CCRC-M25 antibodies recognize β-1,6-linked galactan epitopes from type I or type II arabinogalactan (Ruprecht et al. 2017) in de-arabinosylated RG-I (Wall*Mab*DB). De-arabinosylated RG-I has been detected using CCRC-M22 in the G-layer of gelatinous fibers in gum trees that was thought to be involved in cell swelling and generating force within their tension wood (Bowling and Vaughn 2008). These data suggest galactan-rich

Downloaded from https://academic.oup.com/pcp/article/62/12/1944/6352475 by guest on 21 January 2025

RG-I may strengthen the mature glandular trichome cell wall at the stage of greatest metabolite volume and likely pressure. Based on the observation that the secretory disk surface wall remains as thick as presecretory trichomes despite undergoing delamination and that the CCRC-M22 label is detected in close proximity to the apical PM, we speculate that the secretory trichome walls are reinforced with RG-I that is deposited after cavity biogenesis.

The complementary approach of glycomic analysis with immunolocalization provides the first in-depth investigation of glandular trichome cavity formation in any species. Delamination of the glandular trichome wall occurs in an HG-rich subcuticular wall layer that exhibits a significant decrease in fucosylated xyloglucans, suggesting these components and their modification/degradation play a role in early cavity formation. Small droplets of metabolites are packaged by glycoprotein epitopes within the growing cavity, providing an emulsifying physicochemical interface between the lipophilic metabolites and residual hydrophilic apoplast. Deposition of a distinct subset of RG-I epitopes in mature trichome disk cells may play a role in rigidifying the secretory disk surface wall and/or metabolite backflow reduction from the cavity to the glandular disk cells.

Materials and Methods

Plant material

For all of the plant material in this thesis, cannabis plants were grown in Health Canada permitted space at Anandia Laboratories and Aurora Cannabis Inc. under the supervision of Dr. Jonathan Page. Female pistillate *Cannabis sativa* L. plants of the medicinal-type variety 'Purple Kush' were grown via clonal propagation. Clones were rooted in rockwool and then transferred directly into a soil mixture containing 1.5 tablespoons of Florikote^{TM} (15-5-15) per 1 l of soil (Sungro, Sunshine Mix #4). Plants were grown in a growth chamber (BC Northern Lights) under LED lights (BC Northern lights, 3,000 K 80 CRI spectrum). Plants were watered with tap water for the first 2 weeks after planting and subsequently water with Peter's Excel® (15-5-15) at a concentration of 0.05 tablespoons per liter for the duration of vegetative growth. Sterile bamboo stakes were used to support plant weight to best maintain an upright position when necessary. For biological controls, *Phytoseiulus persimilis* was applied to the plants on a weekly basis, as well as bi-weekly treatments of *Neoseiulus cucumeris* and *Amblydromalus limonicus* for the duration of vegetative and floral development. The plants were subjected to vegetative growth for 2–3 weeks using an 18 h/6 h light cycle and watered with Peter's Excel® (15-5-15). To induce flower development, the light cycle was switched to 12/12 and plants were watered with Maxibloom (5-15-14).

Glandular trichome preparation and isolation

Glandular trichomes were isolated from cannabis flowers as described in detail previously (Livingston et al. 2020). Briefly, 7 g of cannabis floral clusters were harvested from three independent week 6 flowering 'Purple Kush' plants (total 21 g of floral clusters). Flowers were excised with scissors and cooled to 4°C in isolation buffer (0.6% w/v methyl cellulose, 1% w/v PVP^3 MW 40,000, 25 mM HEPES, 200 mM sorbitol, 10 mM sucrose, 10 mM KCl, 5 mM $MgCl_2$-$6H_20$ and 0.5 mM KH_2PO_4) with Amberlite XAD4 beads (1 g g^{-1} plant material; Sigma). All subsequent steps were performed at 4°C. Plant material was blended with short pulses in a blending chamber and filtered through 250 μm nylon mesh to remove large plant debris and Amberlite beads and then rinsed with cold wash buffer (same composition as isolation buffer, except methyl cellulose and PVP^3). The filtrate was then filtered through 202 μm nylon mesh to remove the majority of stalks, epidermal fragments and non-glandular trichomes and subsequently washed with cold wash buffer. The filtrate was then passed through a 54 μm nylon mesh, which filtered out glandular trichome heads with minor contamination from non-glandular trichomes. Trichomes were collected from the mesh surface using a wide-bore 5 ml transfer pipette and wash buffer. Trichomes sedimented in round-bottom tubes (Fisher Scientific 14-959-10B) over 30 min incubated on ice. At the end of the trichome preparation, three vegetative leaves were harvested from each of three plants for a total of nine vegetative leaves. Leaves were placed on ice for 30 min.

Glycome profiling

Trichome preparations (~1 ml sedimented gland heads) and vegetative leaves (1.5 g fresh weight) were transferred to 50 ml falcon tubes with thirty 20 mm stainless steel beads and the remaining volume filled with distilled water. Tubes were vortexed for 7 min to pulverize the tissue. Beads and remaining tissue were filtered out from the homogenate using 250 μm mesh. Disrupted cellular debris was centrifuged for 10 m at 4,000 RPM. Supernatant was decanted and replaced with 50 ml 80% EtOH. Tubes were stirred overnight at room temperature on a rotary shaker and then centrifuged at 3,000×*g* for 15 min. Supernatant was decanted and the pellets washed with anhydrous EtOH once and anhydrous acetone twice. The resulting cell wall AIR was vacuum dried for 24 h at room temperature. To generate sufficient AIR from glandular trichomes, AIR preparation was performed three times and the resulting AIR from all three replicates were pooled for downstream analysis. The following steps for cell wall extraction and preparation for glycomic analysis were performed based on previously described methods, where detailed information on each step can be found (Pattathil et al. 2012). The AIR for isolated glandular trichome heads and vegetative leaves was sequentially extracted using 50 mM ammonium oxalate, 50 mM sodium carbonate, 1 M KOH and 4 M KOH. Total sugars of each fraction were estimated using a phenol-sulfuric acid microplate assay (Masuko et al. 2005). ELISAs were performed with 155 cell wall-directed monoclonal antibodies (Pattathil et al. 2010) against each wall fraction. ELISA responses were graphically represented as a heat map using a modified version of R-Console software.

Monosaccharide analysis

Trichome preparations (sedimented gland heads) and vegetative leaves were ground in liquid nitrogen and ~60–80 mg of sample was transferred to O-ring screw cap vials. Samples were subjected to extraction with hexane, chloroform, ethanol, water and acetone. The first three extractions were placed in a sonication bath for 30 min at room temperature followed by centrifugation for 5 min at 9,000 rpm. Water and acetone extractions were performed at 100°C and 60°C, respectively, in a thermomixer, followed by centrifugation for 3 min at 9,000 rpm. Pellets were dried overnight at 50°C.

Dry wall residues were subjected to hydrolysis using either a modified Klason procedure or a 2 M trifluoroacetic acid (TFA) hydrolysis. Briefly, for the modified Klason procedure, 3–5 mg of tissue was incubated with 50 μl of 72% sulfuric acid for 1 h at 30°C in a thermomixer at 500 rpm. After 1 h, 1 ml of ultrapure water was added to the samples and autoclaved at 121°C for 60 min. Samples were cooled down, spun for 5 min at 12,000 rpm, and supernatant was collected and stored at 4°C. A second set of samples were hydrolyzed using 1 ml of 2 M TFA and autoclaved at 121°C for 60 min. Samples were cooled, spun for 5 min at 12,000 rpm and supernatant was collected and stored at 4°C.

Monomeric neutral and acid carbohydrate composition was analyzed in an Agilent 1290 UHPLC with a diode array detector (Agilent Technologies Inc. CA, USA). Hydrolyzed samples were subjected to a modified labeling protocol described by Sakamoto et al. (2015). An aliquot (80 μl) of the hydrolysate and 10 μl of internal standard (3-O-methyl-glucose 10 mg/ml) were incubated

Downloaded from https://academic.oup.com/pcp/article/62/12/1944/6352475 by guest on 21 January 2025

with 80 μl of the labeling reagent (benzocaine 100 mg/ml, glacial acetic acid 117 μl/ml and sodium cyanoborohydride 10 mg/ml) for 1 h at 60°C. Samples were then cooled, diluted in methanol and filtered before analysis in the UHPLC. Separation of sugars was obtained in the AQUITY BEH C18 column (Waters Inc., MA, USA). Column was maintained at 50°C. Concentration of neutral and acid sugars was based on a standard curve calibration.

High-pressure freezing and freeze-substitution

Purple Kush floral clusters from week 3 (early flowering), week 5 (mid-stage flowering) and week 8 (late-stage flowering) of three cannabis plants were harvested to capture glandular trichomes of all stages of development. Individual florets were dissected and hand-sectioned to generate cylindrical cross-sections that were < 3 mm in diameter and ∼0.5 mm in height. Tissue cross-sections were immersed in hydrated baker's yeast or hexadecane as a cryoprotectant and loaded into high-pressure freezing cartridges. Samples were frozen with a high-pressure freezer (Leica HPM100) and transferred to a liquid nitrogen storage dewar.

Samples for ultrastructural analysis were transferred to a freeze-substitution vial containing 2% (w/v) osmium tetroxide and 8% (v/v) dimethoxypropane in anhydrous acetone and freeze-substituted for 5 d at −80°C in a chest freezer. Samples were transferred to −20°C for 24 h, followed by 4°C for 2 h and, finally, room temperature for 2 h. Samples were separated from their freezing cartridge and rinsed five times in anhydrous acetone. Spurr's resin (Electron Microscopy Services) was gradually infiltrated in an ascending series of 10, 20, 40, 60, 80, 95, and 100% resin for at least 3 h each. Two additional 100% resin exchanges were performed for 24 h each, and then samples were transferred to Beem capsules (Ted Pella) containing fresh 100% Spurr's resin and polymerized at 60°C for 48 h.

Samples for immunolabeling were transferred to a freeze-substitution vial containing 0.25% (v/v) glutaraldehyde, 0.1% (w/v) uranyl acetate and 8% (v/v) dimethoxypropane. All following freeze-substitution and resin-embedding steps were performed in an automatic freeze-substitution machine (Leica AFS2). Samples were substituted over 4 d at −80°C. Samples were warmed to −50°C over 24 h and then separated from their freezing cartridge and exchanged with anhydrous acetone twice. HM20 resin (Electron Microscopy Sciences) was gradually infiltrated in an ascending series of 10, 20, 40, 60, 80, and 100% resin for 8 h at each step. Two additional 100% resin exchanges were performed for 8 h each, then samples were polymerized under UV light at −50°C for 36 h. After polymerization, samples were warmed to 4°C over 12 h and then to room temperature over 2 h.

Ultrastructure TEM

Two blocks from each of three independent freezes were prepared for ultrastructural analysis. Spurr's-embedded samples were sectioned using a Leica UCT Ultramicrotome. 70 nm ultra-thin sections were cut with a diamond knife and mounted on copper grids coated with 0.3% formvar. Sections were post-stained with 2% aqueous uranyl acetate and lead citrate for 10 and 5 min, respectively. Imaging of sections was performed using a Hitachi 7600 transmission electron microscope operating at 80 kV. Images were acquired using an AMT XR51 CCD camera.

Antibody-specific information

A list of all primary antibodies/probes tested in this manuscript, their source reference, supplier and qualitative labeling pattern in cannabis calyces are summarized in **Supplementary Table S2**. All CCRC-series antibodies and anti-callose antibody are monoclonal antibodies derived from mouse IgG. All LM-series and JIM-series antibodies are monoclonal antibodies derived from rat IgG. The CBM3a probe contains a carbohydrade-binding motif and poly-histidine tag, which is recognized by the mouse anti-HIS monoclonal antibody (MA1-21315; ThermoFisher).

Immunofluorescence labeling, imaging and quantification

Two blocks from each of three independent freezes (six total) were prepared for antibody labeling. HM20-embedded samples were sectioned using a Leica UCT Ultramicrotome. 350 nm thin sections were cut with a glass knife and mounted onto 10-well PTFE glass slides coated with 0.1% poly-L-lysine. Sections were blocked in 5% w/v non-fat dry milk (NFDM) in TBS-T for 30 min at room temperature, followed by a rinse step (thoroughly washed in a constant flow of TBS-T for 1 min). All primary antibodies were prepared at a 1:5 dilution in TBS-T containing 1% NFDM for 1 h at room temperature, with the exception of the CBM probe (1:5 polyhistidine-tagged CBM3a for 1 h, followed by 1:1,000 mouse anti-HIS for 1 h), followed by a rinse step. All secondary antibodies (Alexa 488 goat anti-rat; Alexa 488 goat anti-mouse, ThermoFisher) were prepared at a 1:100 dilution in TBS-T containing 1% NFDM for 1 h at room temperature, followed by a rinse step. Immunolabeled sections were rinsed in distilled water for 5 min then mounted in 100% glycerol and a coverslip. Two slides of primary antibody controls for each of the six blocks were prepared (no primary antibody, Alexa 488 anti-rat secondary; no primary antibody, Alexa 488 anti-mouse secondary) for the preliminary assessment of antibody specificity. Two independent rounds of immunolabeling for each antibody were performed.

Immunofluorescence imaging was performed at room temperature using a Perkin–Elmer UltraView VoX spinning disk confocal microscope mounted on a Leica DMi8 inverted microscope with a Hamamatsu 9100-02 CCD camera using the 488 laser line and GFP emission filter cube. Sections were imaged using a 20×, 40× or 63× objective during preliminary screening, and the 63× objective exclusively for images used in fluorescence quantification. Imaging parameters were optimized for each individual primary antibody based on a scan of all sections labeled with a particular antibody by setting the laser intensity and brightness (gain) to capture the most intense pixels at saturation. This setting was used consistently for all images of an antibody. Exposure time was constant at 300 ms for all antibodies. Images were acquired using Volocity image analysis software on the confocal microscope.

Image processing and quantification was performed using FIJI (Fiji Is Just ImageJ). Image stacks were processed into Z-projections with maximum intensity. Fluorescence signal was converted into a heat map of pixel intensity using the lookup table 'Fire'. Using the selection brush tool set to 2 pixel width, regions of interest (ROI) within an image were selected for pixel intensity measurements, capturing area and integrated density (ID) measurements. Mean pixel intensity for an ROI was determined by the sum of ID/sum of area across the entire wall domain of interest. Reported fluorescence measurements corresponds to the mean pixel intensity of an ROI subtracted by background intensity for the image it was derived from. For each image, the mean pixel intensity of five ROIs were selected in the vacuoles of epidermal cells or the glandular trichome disk as a measurement of background fluorescence. Epidermal wall measurements correspond to traces of the apical wall domain of all epidermal cells visible within an image. Presecretory apical wall domains correspond to the apical wall domains bound by the ellipsoid periclinal vertices. Subcuticular wall domains correspond to the subcuticular sheath of secretory stage trichomes that had delaminated from the secretory disk surface wall. Delamination zones correspond to areas at the junction between subcuticular wall domains and secretory disk surface walls where there was evidence of wall expansion and conspicuous small metabolite droplets but not complete separation. Secretory disk surface wall domains correspond to the wall domain that remains contiguous with the PM after delamination. Intercompartmental walls correspond to the intracavity wall fibrils between the subcuticular and disk cell surface domains that surround cavity droplets.

Presecretory trichomes were defined by the absence of evidence for cavity formation within a cross-section, and their basal wall domain was within 10 μm of the epidermal plane. Secretory stage trichomes were defined by evidence of cavity formation (subcuticular wall was separated from the disk cell surface). Mature glandular trichomes were defined by evidence of cavity formation, and

Downloaded from https://academic.oup.com/pcp/article/62/12/1944/6352475 by guest on 21 January 2025

either the presence of a stalk of > 40 μm or the basal domain of the trichome was > 40 μm above the epidermal plane (trichomes that likely possess a stalk that is outside the plane of section).

Statistical comparisons were performed using Statistical Package for Social Sciences v25.0. Fluorescence measurements were graphed using a dot plot in Microsoft Excel.

ImmunoTEM labeling and counting

Two blocks from two independent freeze replicates (four total blocks) were prepared for antibody labeling. HM20-embedded samples were sectioned using a Leica UCT Ultramicrotome. 70 nm ultra-thin sections were cut with a diamond knife and mounted onto nickel grids coated with 0.3% formvar. Sections were blocked in 5% w/v NFDM in TBS-T for 60 min at room temperature, followed by a rinse step (thoroughly washed in a constant flow of TBS-T for 1 min). All primary antibodies were prepared at a 1:5 dilution in TBS-T containing 1% NFDM for 1 h at room temperature, followed by a rinse step. 10 nm colloidal gold anti-mouse antibodies (Ted Pella) were prepared at a 1:100 dilution in TBS-T containing 1% NFDM for 1 h at room temperature, followed by a rinse step. Immunolabeled sections were rinsed in distilled water for 5 min then dried completely. Sections were post-stained in 2% uranyl acetate and lead citrate for 5 and 2 min, respectively. For each biological replicate, a no primary antibody 10 nm colloidal gold anti-mouse secondary antibody was used as a control. One round of immunolabeling for each antibody was performed.

For the gold particle counting performed in **Figs. 4** and **5**, four total trichomes were imaged from two blocks containing presecretory and early secretory trichomes for each antibody. Two images were acquired for each trichome, and all gold particles present within the images were counted based on the criteria that follows. Presecretory apical walls were defined as a domain between the periclinal ellipsoid vertices of the presecretory glandular trichome head cross-section. For epitope distribution analysis, gold particles present within cell corners were omitted. Delamination zones were defined by the presence of conspicuous porosity in the apical wall domains between the PM and the cuticle. The normalized distance of the gold particle from the apical PM was determined by measuring the distance from the PM divided by the distance from PM to cuticle. The PM-cuticle measurement was performed for each gold particle by drawing a perpendicular line from the PM through each respective gold particle to normalize for variation in wall thickness. The normalized distance of gold particles from PM was binned into deciles to compare distribution of epitopes between trichome developmental stages.

For gold particle counting performed in **Fig. 9**, seven total trichomes were imaged from two blocks containing stalked glandular trichomes (>40 μm stalk length or > 40 μm distance between basolateral domain of glandular head from calyx epidermal cuticle) without compartmentalization in the cross-section. Three or more images of each trichomes secretory surface wall were imaged. Gold particle distance from PM was determined by measuring a perpendicular line from PM to gold particle. Gold particles present in the cell corners were omitted from distance analysis.

Cuticle and cell wall thickness measurements

TEM micrographs of glandular trichomes acquired from three separate freezes were used for measuring the cuticle and cell wall thickness. Presecretory trichomes were defined by the absence of evidence for cavity formation within a cross-section, and their basal wall domain was within 10 μm of the epidermal plane. Secretory stage trichomes were defined by evidence of cavity formation (subcuticular wall was separated from the disk cell surface wall). All reported wall and cuticle thickness measurements are the average of five measurements for each domain measured from each trichome. Wall thickness measurements were only performed where the cell wall lamellae were continuous (no conspicuous metabolite droplets separating wall lamellae within the domain of interest; example measurements in **Fig. 8**).

Supplementary Data

Supplementary data are available at PCP online.

Data Availability

The data underlying this article will be shared on request to the corresponding author.

Funding

Canadian Natural Sciences and Engineering Research Council Discovery Grant (RGPIN-2019-04592 to A.L.S.); a Plant Genome Program NSF grant (IOS-0923992 to M.G.H.).

Acknowledgements

The authors would like to thank Dr. Jonathon Briggs and Dr. Harry Brumer for their thoughtful discussion of the manuscript and Sivasankari Venkatachalam (University of Georgia) for the glycome profiling data. The efforts of many Aurora Cannabis Inc. employees involved in plant cultivation and maintenance through the duration of the project are greatly appreciated, as well as the UBC Bioimaging Facility (RRID:SCR_021304) for its technical assistance.

Disclosures

Jonathan E. Page was the CSO of Aurora Cannabis Inc., a cannabis licensed producer and biotechnology company, at the time of data collection.

References

Anderson, C.T. and Kieber, J.J. (2020) Dynamic construction, perception, and remodeling of plant cell walls. *Annu. Rev. Plant Biol.* 71: 39–69.

Bergau, N., Bennewitz, S., Syrowatka, F., Hause, G. and Tissier, A. (2015) The development of type VI glandular trichomes in the cultivated tomato Solanum lycopersicum and a related wild species S. Habrochaites. *BMC Plant Biol.* 15: 289.

Bidhendi, A.J. and Geitmann, A. (2016) Relating the mechanics of the primary plant cell wall to morphogenesis. *J. Exp. Bot.* 67: 449–461.

Bleeker, P.M., Diergaarde, P.J., Ament, K., Guerra, J., Weidner, M., Schütz, S., et al. (2009) The role of specific tomato volatiles in tomato-whitefly interaction. *Plant Physiol.* 151: 925–935.

Bleeker, P.M., Diergaarde, P.J., Ament, K., Schütz, S., Johne, B., Dijkink, J., et al. (2011) Tomato-produced 7-epizingiberene and R-curcumene act as repellents to whiteflies. *Phytochemistry* 72: 68–73.

Bowling, A.J. and Vaughn, K.C. (2008) Immunocytochemical characterization of tension wood: gelatinous fibers contain more than just cellulose. *Am. J. Bot.* 95: 655–663.

Cosgrove, D.J. (2016) Plant cell wall extensibility: connecting plant cell growth with cell wall structure, mechanics, and the action of wall-modifying enzymes. *J. Exp. Bot.* 67: 463–476.

Cosgrove, D.J. (2018) Diffuse growth of plant cell walls. *Plant Physiol.* 176: 16–27.

Daher, F.B. and Braybrook, S.A. (2015) How to let go: pectin and plant cell adhesion. *Front. Plant Sci.* 6: 523.

Downloaded from https://academic.oup.com/pcp/article/62/12/1944/6352475 by guest on 21 January 2025

Evans, M., Ratcliffe, I. and Williams, P.A. (2013) Emulsion stabilisation using polysaccharide–protein complexes. *Curr. Opin. Colloid Interface Sci.* 18: 272–282.

Francis, K.E., Lam, S.Y. and Copenhaver, G.P. (2006) Separation of arabidopsis pollen tetrads is regulated by QUARTET1, a pectin methylesterase gene. *Plant Physiol.* 142: 1004–1013.

Funami, T., Zhang, G., Hiroe, M., Noda, S., Nakauma, M., Asai, I., et al. (2007) Effects of the proteinaceous moiety on the emulsifying properties of sugar beet pectin. *Food Hydrocoll.* 21: 1319–1329.

Glas, J.J., Schimmel, B.C.J., Alba, J.M., Escobar-Bravo, R., Schuurink, R.C. and Kant, M.R. (2012) Plant glandular trichomes as targets for breeding or engineering of resistance to herbivores. *Int. J. Mol. Sci.* 13: 17077–17103.

Hammond, C.T. and Mahlberg, P.G. (1978) Ultrastructural development of capitate glandular hairs of *Cannabis sativa* L. (Cannabaceae). *Am. J. Bot.* 65: 140–151.

He, X., Sun, Y. and Zhu, R.L. (2013) The oil bodies of liverworts: unique and important organelles in land plants. *CRC Crit. Rev. Plant Sci.* 32: 293–302.

Huang, C.Y., Chung, C.I., Lin, Y.C., Hsing, Y.I.C. and Huang, A.H.C. (2009) Oil bodies and oleosins in physcomitrella possess characteristics representative of early trends in evolution. *Plant Physiol.* 150: 1192–1203.

Huchelmann, A., Boutry, M. and Hachez, C. (2017) Plant glandular trichomes: natural cell factories of high biotechnological interest. *Plant Physiol.* 175: 6–22.

Jeffree, C.E. (2006) The fine structure of the plant cuticle. *In* Annual Plant Reviews Volume 23: Biology of the Plant Cuticle. Edited by Riederer, M. and Müller, C. pp. 11–125. Blackwell Publishing Ltd, Oxford, UK.

Johnson, K.L., Cassin, A.M., Lonsdale, A., Wong, G.K.S., Soltis, D.E., Miles, N.W., et al. (2017) Insights into the evolution of hydroxyproline-rich glycoproteins from 1000 plant transcriptomes. *Plant Physiol.* 174: 904–921.

Jones, L., Milne, J.L., Ashford, D. and McQueen-Mason, S.J. (2003) Cell wall arabinan is essential for guard cell function. *Proc. Natl. Acad. Sci.* 100: 11783–11788.

Livingston, S.J., Quilichini, T.D., Booth, J.K., Wong, D.C.J., Rensing, K.H., Laflamme-Yonkman, J., et al. (2020) Cannabis glandular trichomes alter morphology and metabolite content during flower maturation. *Plant J.* 101: 37–56.

Masuko, T., Minami, A., Iwasaki, N., Majima, T., Nishimura, S.I. and Lee, Y.C. (2005) Carbohydrate analysis by a phenol–sulfuric acid method in microplate format. *Anal. Biochem.* 339: 69–72.

Merelo, P., Agustí, J., Arbona, V., Costa, M.L., Estornell, L.H., Gómez-Cadenas, A., et al. (2017) Cell wall remodeling in abscission zone cells during ethylene-promoted fruit abscission in citrus. *Front. Plant Sci.* 8: 126.

Mikshina, P.V., Idiyatullin, B.Z., Petrova, A.A., Shashkov, A.S., Zuev, Y.F. and Gorshkova, T.A. (2015) Physicochemical properties of complex rhamnogalacturonan I from gelatinous cell walls of flax fibers. *Carbohydr. Polym.* 117: 853–861.

Mohnen, D. (2008) Pectin structure and biosynthesis. *Curr. Opin. Plant Biol.* 11: 266–277.

Morris, G.A., Ralet, M.C., Bonnin, E., Thibault, J.F. and Harding, S.E. (2010) Physical characterisation of the rhamnogalacturonan and homogalacturonan fractions of sugar beet (Beta vulgaris) pectin. *Carbohydr. Polym.* 82: 1161–1167.

Nuñez, A., Fishman, M.L., Fortis, L.L., Cooke, P.H. and Hotchkiss, A.T. (2009) Identification of extensin protein associated with sugar beet pectin. *J. Agric. Food Chem.* 57: 10951–10958.

Ogawa, M., Kay, P., Wilson, S. and Swain, S.M. (2009) ARABIDOPSIS DEHISCENCE ZONE POLYGALACTURONASE1 (ADPG1), ADPG2, and QUARTET2 are polygalacturonases required for cell separation during reproductive development in arabidopsis. *Plant Cell* 21: 216–233.

Padala, S.R., Williams, P.A. and Phillips, G.O. (2009) Adsorption of Gum Arabic, egg white protein, and their mixtures at the oil—water interface in limonene oil-in-water emulsions. *J. Agric. Food Chem.* 57: 4964–4973.

Park, J., Cui, Y. and Kang, B.H. (2015) AtPGL3 is an Arabidopsis BURP domain protein that is localized to the cell wall and promotes cell enlargement. *Front. Plant Sci.* 6: 412.

Pattathil, S., Avci, U., Baldwin, D., Swennes, A.G., McGill, J.A., Popper, Z., et al. (2010) A comprehensive toolkit of plant cell wall glycan-directed monoclonal antibodies. *Plant Physiol.* 153: 514–525.

Pattathil, S., Avci, U., Miller, J.S. and Hahn, M.G. (2012) Immunological approaches to plant cell wall and biomass characterization: Glycome Profiling. *Methods Mol. Biol.* 908: 61–72.

Pérez-Pérez, Y., Carneros, E., Berenguer, E., Solís, M.T., Bárány, I., Pintos, B., et al. (2019) Pectin De-methylesterification and AGP increase promote cell wall remodeling and are required during somatic embryogenesis of quercus suber. *Front. Plant Sci.* 9.

Prasanna, V., Prabha, T.N. and Tharanathan, R.N. (2007) Fruit ripening phenomena–an overview. *Crit. Rev. Food Sci. Nutr.* 47: 1–19.

Pyc, M., Cai, Y., Greer, M.S., Yurchenko, O., Chapman, K.D., Dyer, J.M., et al. (2017) Turning over a new leaf in lipid droplet biology. *Trends Plant Sci.* 22: 596–609.

Ruprecht, C.R., Bartetzko, M.P., Senf, D., Dallabernadina, P., Boos, I., Andersen, M.C.F., et al. (2017) A synthetic glycan microarray enables epitope mapping of plant cell wall glycan-directed antibodies. *Plant Phys.* 175: 1094–1104.

Sakamoto, S., Yoshida, K., Sugihara, N. and Mitsuda, N. (2015) Development of a new high-throughput method to determine the composition of ten monosaccharides including 4-*O*-methyl glucuronic acid from plant cell walls using ultra-performance liquid chromatography. *Plant Biotechnol.* 32: 55–63.

Scheller, H.V. and Ulvskov, P. (2010) Hemicelluloses. *Annu. Rev. Plant Biol.* 61: 263–289.

Schuurink, R. and Tissier, A. (2020) Glandular trichomes: micro-organs with model status? *New Phytol.* 225: 2251–2266.

Siew, C.K. and Williams, P.A. (2008) Role of protein and ferulic acid in the emulsification properties of sugar beet pectin. *J. Agric. Food Chem.* 56: 4164–4171.

Simmons, A.T. and Gurr, G.M. (2005) Trichomes of Lycopersicon species and their hybrids: effects on pests and natural enemies. *Agric. For. Entomol.* 7: 265–276.

Sirikantaramas, S., Taura, F., Tanaka, Y., Ishikawa, Y., Morimoto, S. and Shoyama, Y. (2005) Tetrahydrocannabinolic acid synthase, the enzyme controlling marijuana psychoactivity, is secreted into the storage cavity of the glandular trichomes. *Plant Cell Physiol.* 46: 1578–1582.

Tissier, A., Morgan, J.A. and Dudareva, N. (2017) Plant volatiles: going 'in' but not 'out' of trichome cavities. *Trends Plant Sci.* 22: 930–938.

Verhertbruggen, Y., Marcus, S.E., Haeger, A., Verhoef, R., Schols, H.A., McCleary, B.V., et al. (2009) Developmental complexity of arabinan polysaccharides and their processing in plant cell walls. *Plant J.* 59: 413–425.

Wang, D., Samsulrizal, N.H., Yan, C., Allcock, N.S., Craigon, J., Blanco-Ulate, B., et al. (2019) Characterization of CRISPR mutants targeting genes modulating pectin degradation in ripening tomato. *Plant Physiol.* 179: 544–557.

Wang, X., Wilson, L. and Cosgrove, D.J. (2020) Pectin methylesterase selectively softens the onion epidermal wall yet reduces acid-induced creep. *J. Exp. Bot.* 71: 2629–2640.

Willats, W.G., Marcus, S.E. and Knox, J.P. (1998) Generation of monoclonal antibody specific to (1—>5)-alpha-L-arabinan. *Carbohydr. Res.* 308: 149–152.

Willats, W.G.T., Knox, J.P. and Mikkelsen, J.D. (2006) Pectin: new insights into an old polymer are starting to gel. *Trends Food Sci. Technol.* 17: 97–104.

Downloaded from https://academic.oup.com/pcp/article/62/12/1944/6352475 by guest on 21 January 2025

Willats, W.G.T., Steele-King, C.G., Marcus, S.E. and Knox, J.P. (1999) Side chains of pectic polysaccharides are regulated in relation to cell proliferation and cell differentiation. *Plant J.* 20: 619–628.

Williams, P.A., Idris, O.H.M. and Phillips, G.O. (2000) Structural analysis of gum from Acacia Senegal (Gum Arabic). *In* Cell and Developmental Biology of Arabinogalactan-Proteins. Edited by Nothnagel, E.A., Bacic, A. and Clarke, A.E. pp. 241–251. Springer US, New York, USA.

Witasari, L.D., Huang, F.C., Hoffmann, T., Rozhon, W., Fry, S.C. and Schwab, W. (2019) Higher expression of the strawberry xyloglucan endotransglucosylase/hydrolase genes FvXTH9 and FvXTH6 accelerates fruit ripening. *Plant J.* 100: 1237–1253.

Yates, E.A., Valdor, J.F., Haslam, S.M., Morris, H.R., Dell, A., Mackie, W., et al. (1996) Characterization of carbohydrate structural features recognized by anti-arabinogalactan-protein monoclonal antibodies. *Glycobiology* 6: 131–139.

Yeats, T.H. and Rose, J.K.C. (2013) The formation and function of plant cuticles. *Plant Physiol.* 163: 5–20.

Zager, J.J., Lange, I., Srividya, N., Smith, A. and Lange, B.M. (2019) Gene networks underlying cannabinoid and terpenoid accumulation in cannabis. *Plant Physiol.* 180: 1877–1897.

Zhang, T., Zheng, Y. and Cosgrove, D.J. (2016) Spatial organization of cellulose microfibrils and matrix polysaccharides in primary plant cell walls as imaged by multichannel atomic force microscopy. *Plant J.* 85: 179–192.

Zheng, L., Heupel, R.C. and DellaPenna, D. (1992) The beta subunit of tomato fruit polygalacturonase isoenzyme 1: isolation, characterization, and identification of unique structural features. *Plant Cell* 4: 1147–1156.

Zheng, L., Watson, C.F. and DellaPenna, D. (1994) Differential expression of the two subunits of tomato polygalacturonase isoenzyme 1 in wild-type and in tomato fruit. *Plant Physiol.* 105: 1189–1195.

Downloaded from https://academic.oup.com/pcp/article/62/12/1944/6352475 by guest on 21 January 2025